TECHNICAL MEMORANDUM

597

Simulation of the MJO and its teleconnections in an ensemble of 46-day EPS hindcasts

F. Vitart and F. Molteni

Research Department

September 2009

European Centre for Medium-Range Weather Forecasts
Europäisches Zentrum für mittelfristige Wettervorhersage
Centre européen pour les prévisions météorologiques à moyen terme

Series: ECMWF Technical Memoranda

A full list of ECMWF Publications can be found on our web site under:
http://www.ecmwf.int/publications/

Contact: library@ecmwf.int

European Centre for Medium-Range Weather Forecasts
Shinfield Park, Reading, RG2 9AX, England

Abstract

A series of 15-member ensemble of 46-day EPS integrations starting on the 15th of each month from 1989 to 2008 has been completed with IFS cycle 32r3. The Madden Julian Oscillation (MJO) simulated by this set of hindcasts is diagnosed using an index based on combined EOFs of zonal winds at 200 and 850 hPa and Outgoing Longwave radiation (OLR). The model is able to maintain the amplitude of the MJO during the 46 days of integrations and it displays skill for up to about 20 days to predict the evolution of the MJO. However, the MJO simulated by the model has a too slow propagation. The impact of the MJO on tropical precipitation and tropical cyclone activity is generally consistent with analysis or observations. The simulated impact of the MJO on the Northern Extratropics weather displays similar patterns as in the analysis (20 years of ERA Interim). However, the impact of the MJO on the 500 hPa geopotential height is generally too strong over the North Pacific, and too weak over the Euro-Atlantic sector. In particular the impact of MJO on the NAO is weaker in the model than in ERA Interim. This problem is consistent with the slow MJO eastward propagation. The MJO simulated by the hindcasts has a significant impact on weekly mean probabilistic skill scores, particularly for the time range day 19-25. At this time range, the reliability of the probabilistic forecasts over Europe depends strongly on the presence of an MJO event in the initial conditions.

1 Introduction

The MJO is the main source of predictability in the Tropics on time scales exceeding one week but less than a season (Madden and Julian, 1971). It has a significant impact on the Indian (Murakami 1976; Yasunari 1979) and Australian monsoon (Hendon and Liebmann 1990). It plays an active role in the onset and development of an El-Niño event (e.g. Kessler and McPhaden 1995) and has an impact on tropical cyclogenesis (Maloney and Hartmann 2000a; Mo 2000; Maloney and Hartmann 2000b). It also impacts the extratropical weather (Ferranti et al 1990; Cassou, 2008). Therefore it is important for a monthly forecasting system to have skill not only in predicting the evolution of the MJO, but also in the simulation of the MJO teleconnections. The goal of the resent paper is to evaluate the skill of a large set of 46-day Ensemble Prediction System (EPS) hindcasts using IFS Cycle 32r3 to simulate MJO events and its teleconnections both in the Tropics and in the Extratropics.

A first goal of this paper it to assess the skill of the dynamical model to predict MJO events. This skill has so far been assessed routinely for each new model cycle using a serial experiment suggested by Peter Webster (Vitart et al, 2007). In those serial experiments, series of 5-member ensemble integrations of 32-day forecasts are performed for each day from 15 December 1992 till 31 January 1993 (46 cases), during the Intensive Observing Period of the Tropical Ocean Global Atmosphere Coupled Ocean-Atmosphere Response Experiment (TOGA COARE). This experimental setup has the advantage of being cheap enough to be performed for each new model cycle, and give a good indication of the progresses of the MJO in the ECMWF model (see example in Bechtold et al, 2008). This experimental setup has also been used for sensitivity studies like the impact of ocean vertical resolution, atmospheric and oceanic initial conditions, horizontal resolution or changes in model physics (Woolnough et al, 2007, Vitart et al, 2007). However the serial experiments cover only one single MJO event. The skill of the model to predict this specific MJO event may not be representative of the general skill of the model. In the present study, a large number of model hindcasts covering a 20 year

period (1989-2008) is used to assess the skill of the 46-day EPS forecasts. This should give a more reliable evaluation of the skill of the model than the serial experiments. However, the cost of those hindcasts is too high to allow an evaluation of each new IFS cycle.

A second goal of this paper is to evaluate the impact of the MJO in the Tropics (precipitation, tropical storms) and Extratropics (North Atlantic Oscillation). Such study would have been difficult before cycle 32R3 (Cy32r3), since the model could not maintain the amplitude of an MJO event for more than a few days. As a consequence, the impact of the MJO would have been too weak. Over the recent years, the representation of the MJO has improved dramatically, thanks mostly to changes in the model's physics introduced in Cy32R3 (Bechtold et al, 2008). Now IFS is able to maintain the amplitude of the MJO for more than 30 days, which makes it possible to evaluate the teleconnections associated to the MJO in the model integrations.

2 Experimental setup

A series of hindcasts has been performed for the 20-year period 1989 to 2008. The hindcasts start on the 15th of each month and are 46 days long in order to cover the full next calendar month. For each starting date, the hindcasts consist of an ensemble of 15 members: a control and 14 perturbed forecasts. The version of IFS used in this experiment is Cy32r3, which was operational from November 2007 until June 2008. As mentioned in the introduction, this version of IFS showed a clear improvement in the representation of the MJO. The configuration of the hindcast is the same as the one used in the operational monthly forecast at ECMWF (Vitart et al, 2008) except for the length of the forecasts (46 days instead of 32 days for operational monthly forecasts). In this configuration, IFS is first integrated for 10 days with a resolution of TL399 (about 50 km resolution) and 62 vertical levels. At day 10 the horizontal resolution is lowered to TL255 (about 80 km resolution) until the end of the forecast. During the first 10 days, IFS is forced by persisted SST anomalies. After day 10, IFS is coupled to the HOPE ocean GCM. The frequency of coupling is 3 hours. The initial conditions are taken from ERA40 (Upppala et al, 2005) until 2001 and from ECMWF operational analysis after 2001. More details about this model configuration can be found in Vitart et al (2008).

3 MJO diagnostic

The Wheeler and Hendon index (Wheeler and Hendon 2004) has been applied to all the model hindcasts, and also to ERA interim (Simmons et al, 2007) over the period 1989-2008 to evaluate the skill of the monthly forecasting system to predict MJO events and also to produce composites for different phases of the MJO. The Wheeler and Hendon index is calculated by projecting the forecasts or analysis on the two dominant combined EOFs of outgoing longwave radiation (OLR), zonal wind at 200 and 850 hPa averaged between 15N and 15S (Fig. 1). The index has been applied to daily anomalies relative to the 1989-2008 climate instead of the absolute value of the field, which should remove the impact of seasonal cycle. In addition, a 120-day running mean has been applied to remove the variability associated to ENSO. The positive (negative) phase of EOF2 describes suppressed (enhanced) convection over the Indian ocean and enhanced (suppressed) convection over the West Pacific. The

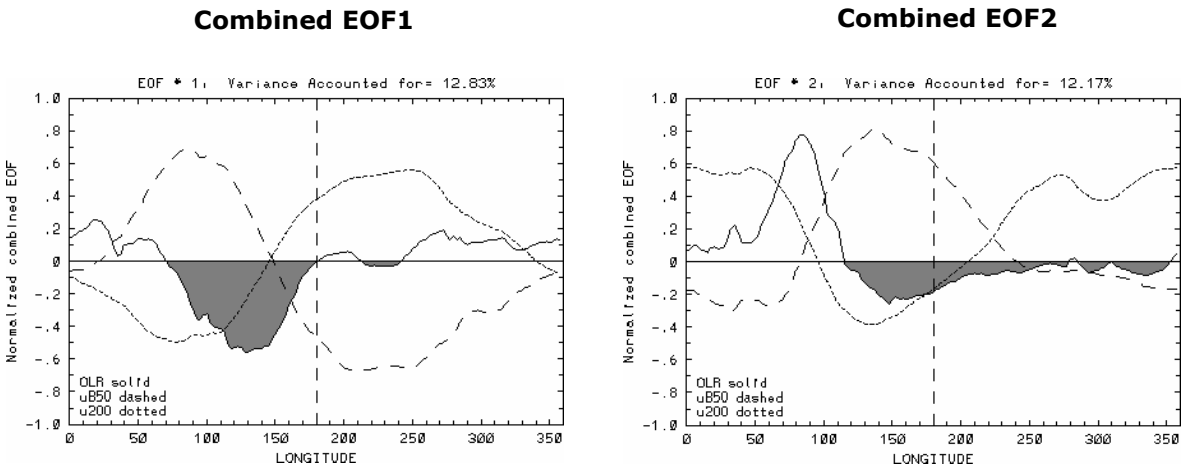

Figure 1: Combined EOF 1 and 2 of OLR, zonal wind at 850 and 200 hPa averaged between 15N and 15S

positive (negative) phase of EOF1 describes enhanced (suppressed) convection over the Maritime Continent region. Analysis and forecasts can be projected onto those two EOFs to describe the phase of the MJO in terms of two time series, PC1 and PC2. The two time series can be plotted as a succession of points in the PC1-PC2 phase space, in such a way that the MJO is described by a clockwise propagation in the phase space (see example in Fig. 2). The PC1-PC2 phase space can be divided into 8 sections representing a specific phase of the MJO (Figure 2). Figure 3 shows a composite of 200 hPa velocity potential for each phase of the MJO using ERA Interim data for the period November to April 1989 to 2008. Phases 2 and 3 (negative EOF2) correspond to enhanced convection over the Indian ocean, phases 4 and 5 (positive EOF1) correspond to the MJO over the Maritime continent, phases 6 and 7 (positive EOF2) correspond to the MJO over the western Pacific and phases 8 and 1 (negative EOF1) correspond to the active phase of the MJO in the western Hemisphere.

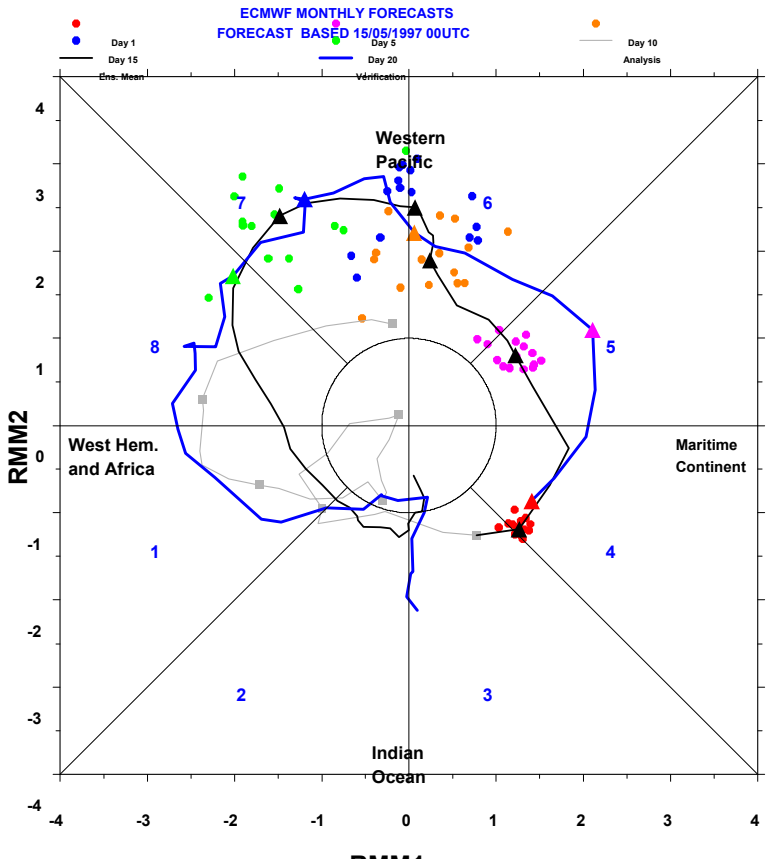

Figure 2: Projection of the 46-day ensemble mean forecast (black line) starting on 15 May 1997 onto the PC1-PC2 phase space. Each circle represents one individual ensemble member for day 1 (red), 5 (magenta), 10 (orange), 15 (blue) and 20 (green). The blue line shows the verification from ERA Interim Reanalysis. The triangles show the verification at day 1,5, 10, 15 and 20. The grey line shows the past 30 day of analysis.

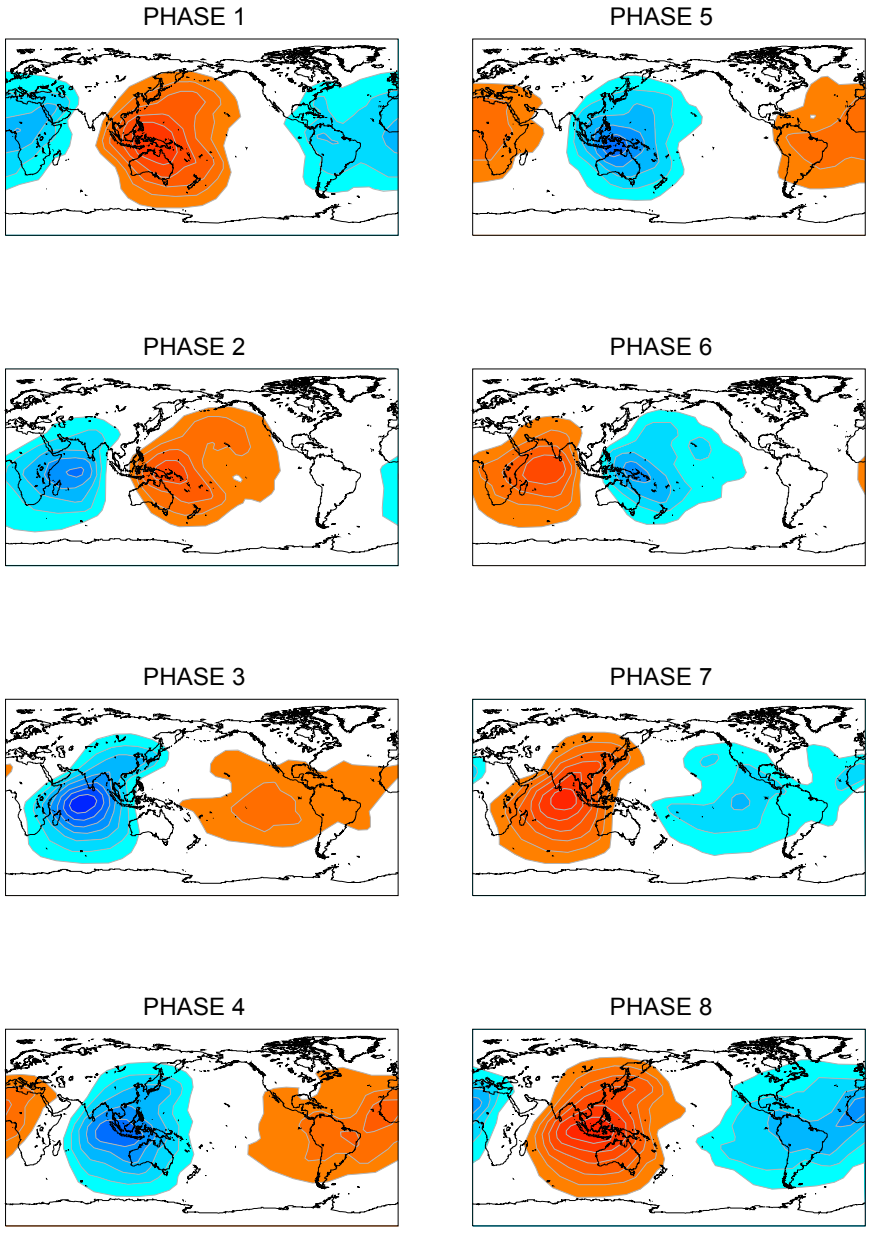

Figure 3: Composites of 200 hPa velocity potential for the 8 phases of the MJO from ERA Interim reanalysis for the period NDJFMA 1989-2008. The blue contours represent negative anomalies and the orange contours represent positive anomalies. The contour interval is $1 \times 10^6\ m^2 s^{-1}$*, and the first contour is* $2 \times 10^6\ m^2 s^{-1}$

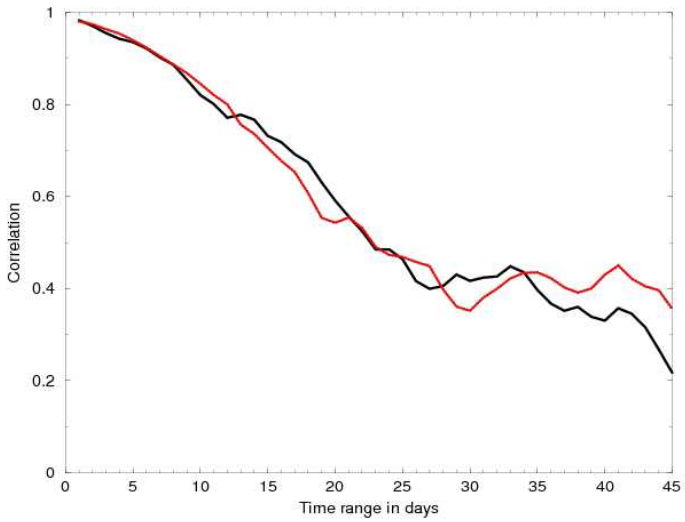

Figure 4: Linear correlation between observed and forecast PC1 (black line) and PC2 (dotted red line) time series as a function of the forecast lead time for the period November to April 1989-2008.

3.1 Skill of the model to predict MJO events

To evaluate the skill of the monthly forecasting system in predicting the MJO, a linear correlation is performed between the observed time series of principal components 1 and 2 with the forecast time series at different lead times. We consider that the forecast is skillful when the anomaly correlation is higher than 0.6.

According to Figures 4, the model has skill to predict the evolution of the MJO up to about day 20. PC1 and PC2 display similar scores. The RMS error of the ensemble mean reaches the RMS error obtained with climatology after day 20 for both PC1 and PC2 (Fig. 5), indicating also useful skill up to day 20.

Figure 6 indicates that the skill of the model is much higher when there is already an MJO in the initial conditions than when there is no MJO in the initial conditions. The skill of the MJO has also been calculated when there is an MJO in the initial conditions in phase 2+3, phase 4+5, phase 6+7 and phase 8+1. According to Figure 7, the skill is higher when there is an MJO over the west Pacific (phase 6+7) in the initial conditions than when there is an MJO over the Indian Ocean in the initial conditions (phase 2+3). Although the number of cases with an MJO in the initial conditions in phase 2+3 or 6+7 is too small to make definitive conclusions, this result is consistent with the difficulty the model has to propagate the MJO across the Maritime continent (see Section 3.3).

Finally, the skill of the model to predict the evolution of the MJO is lower in the period June to September (JJAS) (Fig. 8), when there is less MJO activity than during the period November to April, which corresponds to the period of strong MJO activity. However, in JJAS the correlation drops to

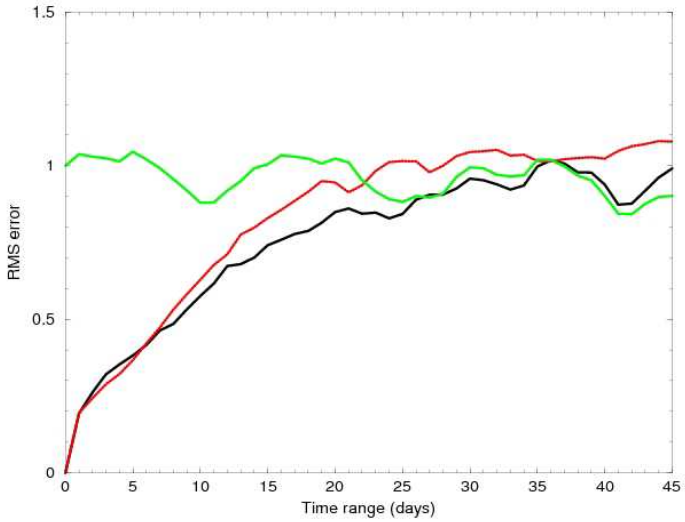

Figure 5: RMS error between ensemble mean PC1 (black line) and PC2 (dotted red line) time series as a function of the forecast lead time for the period November to April. The green line shows the RMS error obtained with climatology.

0.6 around day 20 as for the December to April period.

3.2 Amplitude of the MJO

According to Figure 9, the amplitude of the MJO in IFS starts to increases after day 5 and becomes too strong by about 20% after day 10. Composites of 200 hPa velocity potential and OLR anomalies for the forecast time range day 16-45 confirm the stronger amplitude of the MJO in IFS than in ERA interim (Fig. 10).

3.3 MJO propagation

The monitoring of real-time forecasts from Cy32r3 indicates that the model often fails to propagate the MJO across the Maritime continent, and that it is often too slow over the Indian Ocean (see example in Fig. 11). To check if this is the case in the set of 46-day ensemble hindcasts, a composite of all the MJO events in phase 2 (convection over the west Indian Ocean) has been produced and its daily evolution calculated for the analysis and the ensemble hindcasts. A Hovmoeller diagram of the percentage of cases in a given phase of the MJO shows the eastward propagation of the MJO in both model and analysis, but the propagation is significantly slower in the model than in the reanalysis (Fig. 12). For instance, the majority of MJO events in the reanalysis reach phase 4 within 10 days after

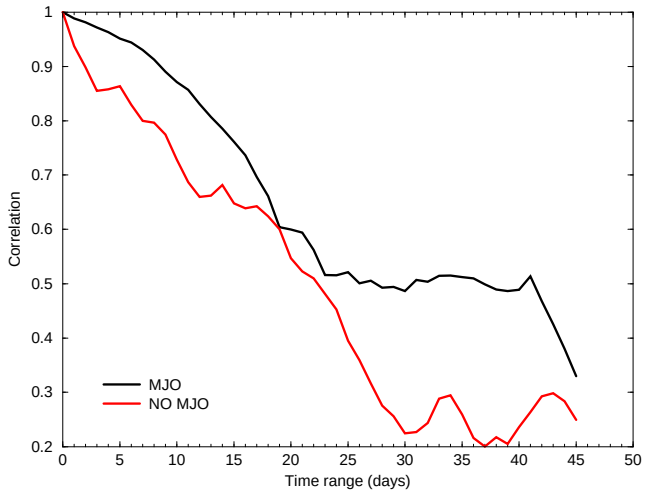

Figure 6: Linear correlation between observed and forecast (PC1+PC2)/2 time series for all the cases with an MJO in the initial conditions (black line) and all the cases without an MJO in the initial conditions (red line) as a function of the forecast lead time for the period November to April.

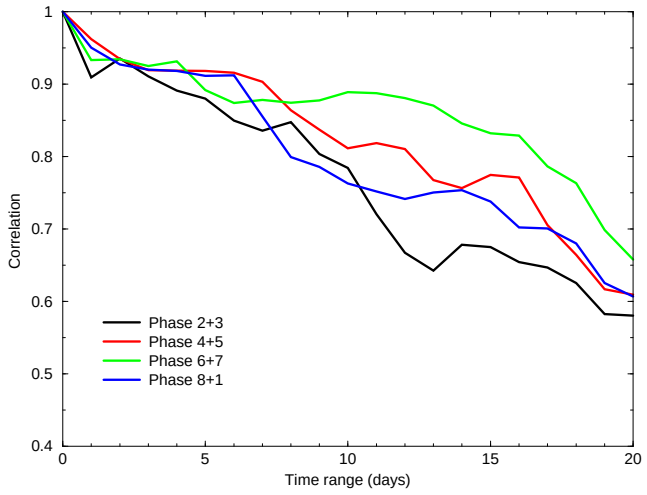

Figure 7: Linear correlation between observed and forecast (PC1+PC2)/2 time series for all the cases with an MJO in phase 2+3,(black line), phase 4+5 (red line), phase 6+7 (green line) and phase (8+1) (blue line) in the initial conditions as a function of the forecast lead time for the period November to April.

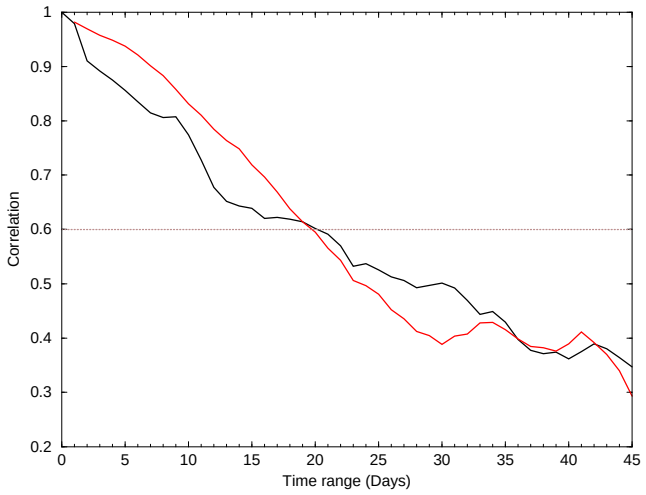

Figure 8: Linear correlation between observed and forecast (PC1+PC2)/2 time series for the period from November to April (black line) and for the period June to September (red line)

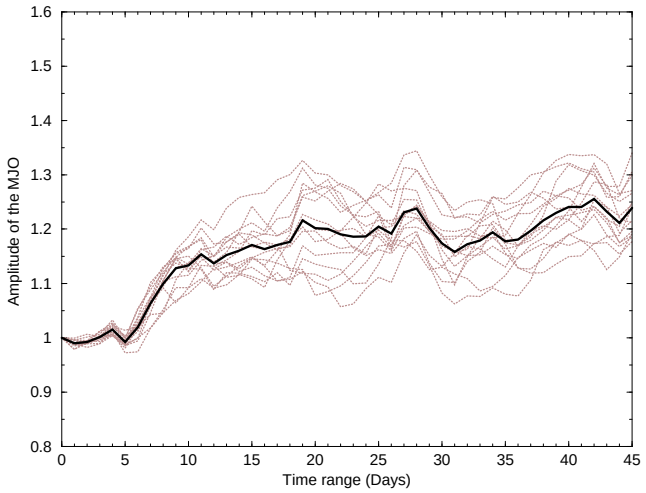

Figure 9: Evolution of the amplitude of (PC1+PC2)/2 as a function of forecast lead time (days) for the period November to April 1989 to 2008. The dotted line represents the amplitude of (PC1+PC2)/2 of individual ensemble members. The solid black line represents the mean amplitude averaged over the 15 ensemble members.

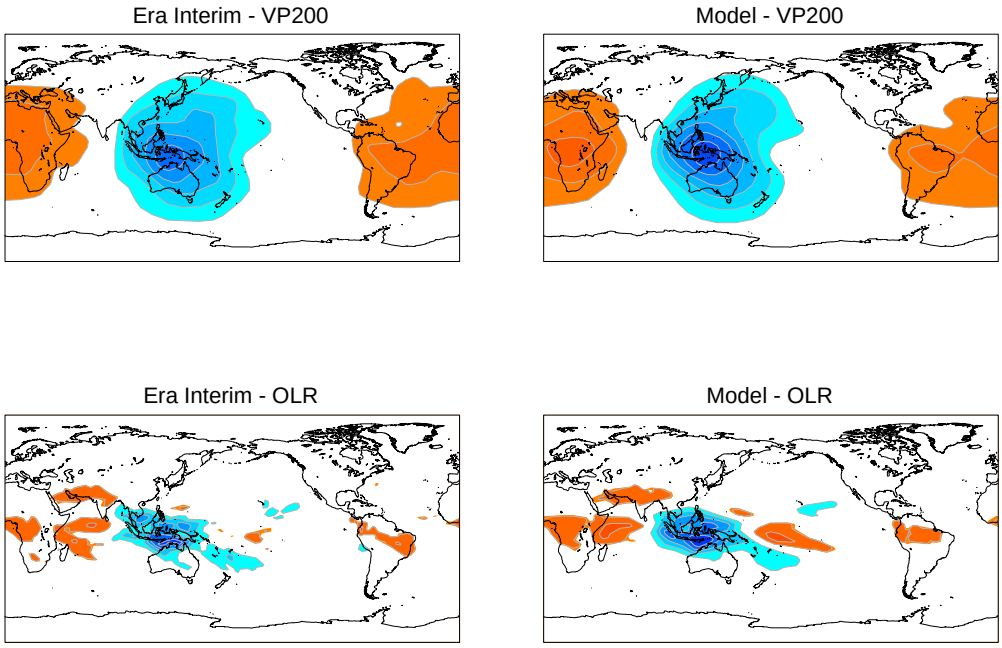

Figure 10: Composites of 200 hPa velocity potential anomalies (top panels) and outgoing longwave radiations (OLR) (bottom panels) from ERA Interim (left panels) and the EPS forecasts (right panels) for the time range day 16-45 and the period November to April 1989 to 2008. For 200 hPa velocity potential, the contour interval is $1 \times 10^6\ m^2 s^{-1}$*, and the first contour is* $2 \times 10^6\ m^2 s^{-1}$*. For OLR, the contour interval is* $5 W m^{-2} s$ *and the first contour interval is* $5 W m^{-2} s$

phase 2, instead of 14 days in the model simulations. This slow propagation of the MJO in the model is confirmed by Figure 13 which shows the time (in number of days) an MJO spends on average in each phase in the analysis (blue bars) and ensemble hindcasts (red bars). Figure 13 confirms that the MJO stays significantly longer in each phase of the MJO in the hindcast than in the analysis, except for phase 5, indicating a much slower propagation in the hindcasts than in the analysis. This slower MJO propagation in the model is not limited to the Indian Ocean, but also takes place over the Pacific and the western Hemisphere.

The percentage of events propagating from one phase of the MJO to the next phase is displayed in Figure 14. The table shows that the percentage of events propagating over the Indian Ocean to the west of the Maritime Continent (from phase 1 to 4) is close in the analysis and in the hindcasts. However, the percentage of MJO events crossing the Maritime continent (phase 4 to 5) and propagating into the west Pacific (phase 5 to 6) is significantly lower in the model than in the reanalysis. In the reanalysis, 30% of MJO events do not propagate from the west part of the Maritime Continent into the western Pacific (from phase 4 to phase 6). This percentage climbs to 50% in the model. This confirms that the model has difficulties to propagate the MJO across the Maritime Continent. On the other hand, the model tends to regenerate too many MJOs from a previous MJO event: in the reanalysis, only 25% of MJOs in phase 7 start a new MJO event over the west Indian Ocean (phase 2). In the model, this percentage climbs to 40%.

4 Teleconnections

This section evaluates the impact of the MJO on various fields in the model and in the ERA Interim reanalysis. The first 15 days of the forecasts have been excluded of the calculation of the composites in order to minimise the impact of initial conditions. In order to reduce the number of panels, phases 2 and 3, 4 and 5, 6 and 7 and 8 and 1 have been merged. Phase 2+3 corresponds to the active phase of the MJO over the Indian Ocean, phase 4+5 corresponds to the MJO over the Maritime continent, phase 6+7 corresponds to the convection over the west Pacific, and phase 8+1 corresponds to the MJO over the western Hemisphere and suppressed convection over the Maritime continent. Phases 2+3 and 6+7 correspond to opposite phases of the MJO. Phases 4+5 and 8+1 represent also opposite phases of the MJO.

4.1 Impact in the Extratropics

4.1.1 Impact on 500 hPa geopotential height anomalies

Figures 15 and 16 show the composites of 500 hPa geopotential height anomalies for phases 2+3, 4+5, 6+7 and 8+1 of the Madden Julian Oscillation in the model hindcasts at the time range day 16-45 and in ERA Interim for the period November to April 1989-2008. The composites are performed only on cases where the amplitude of the MJO index exceeds one standard deviation (outside the central circle in Figure 2) The anomaly patterns are generally consistent between model and reanalysis, but the amplitude of the anomalies can be different in the model and analysis. For instance, the impact of the MJO on the North Pacific sector is weaker (stronger) in the model than in the reanalysis during

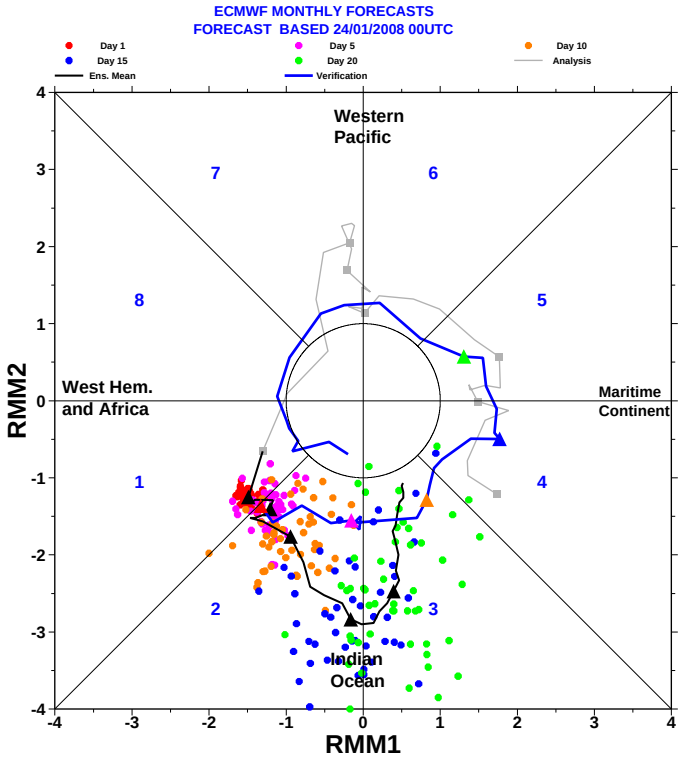

Figure 11: Projection of the 46-day ensemble mean operational forecast (black line) starting on 24 January 2008 onto the PC1-PC2 phase space. Each circle represents one individual ensemble member for day 1 (red), 5 (magenta), 10 (orange), 15 (blue) and 20 (green). The blue line shows the verification from ERA Interim Reanalysis. The triangles show the verification at day 1,5, 10, 15 and 20. The grey line shows the past 30 days of analysis.

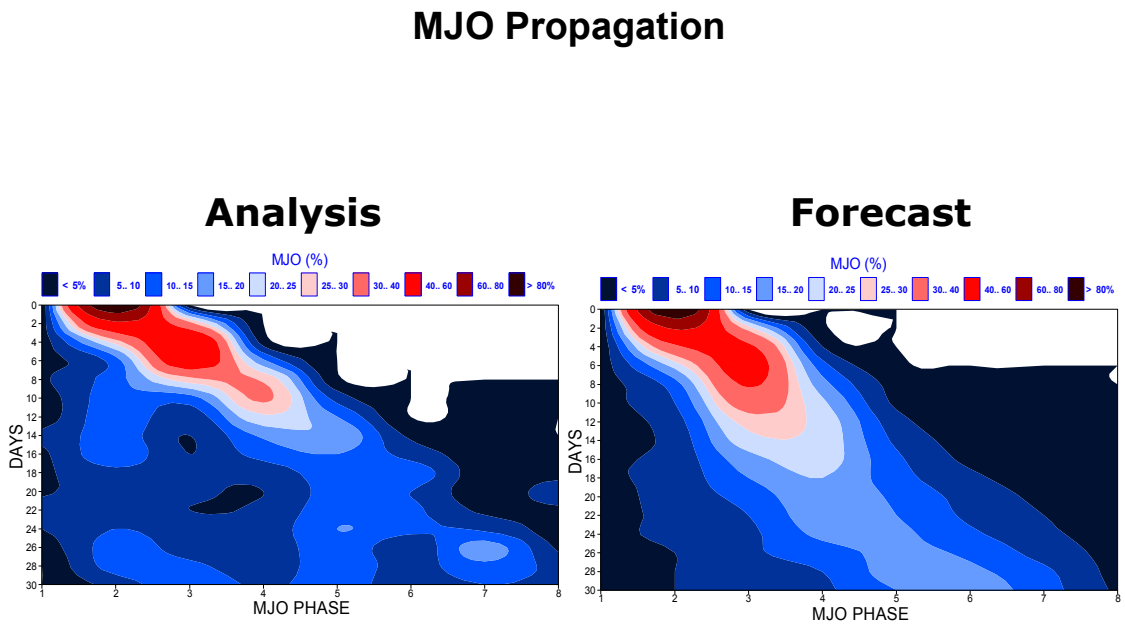

Figure 12: Hovmoeller diagram of the percentage of MJO events in a specific MJO phase as a function of lead time following an MJO in phase 2 (initial time). The left panel shows the eastward propagation in the reanalysis from phase 2, and the right panel shows the eastward propagation of the MJO in the ensemble forecast.

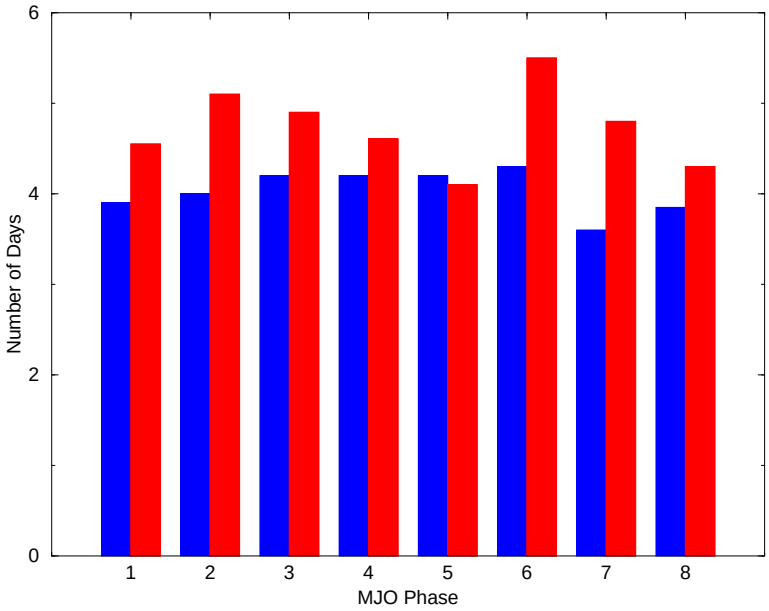

Figure 13: Average number of days an MJO event stays in each of the 8 phases for observations (blue bars) and model hindcasts (red bars).

	Phase 1-> 2	Phase 2-> 3	Phase 3 -> 4	Phase 4 -> 5	Phase 5 -> 6	Phase 6-> 7	Phase 7 -> 8	Phase 8 -> 1
OBS	71%	81%	81%	80%	86%	79%	68%	55%
Model	71%	81%	80%	71%	72%	78%	65%	87%

Figure 14: Percentage of MJO events moving from one MJO phase to another for observations (top row) and model hindcasts (bottom row).

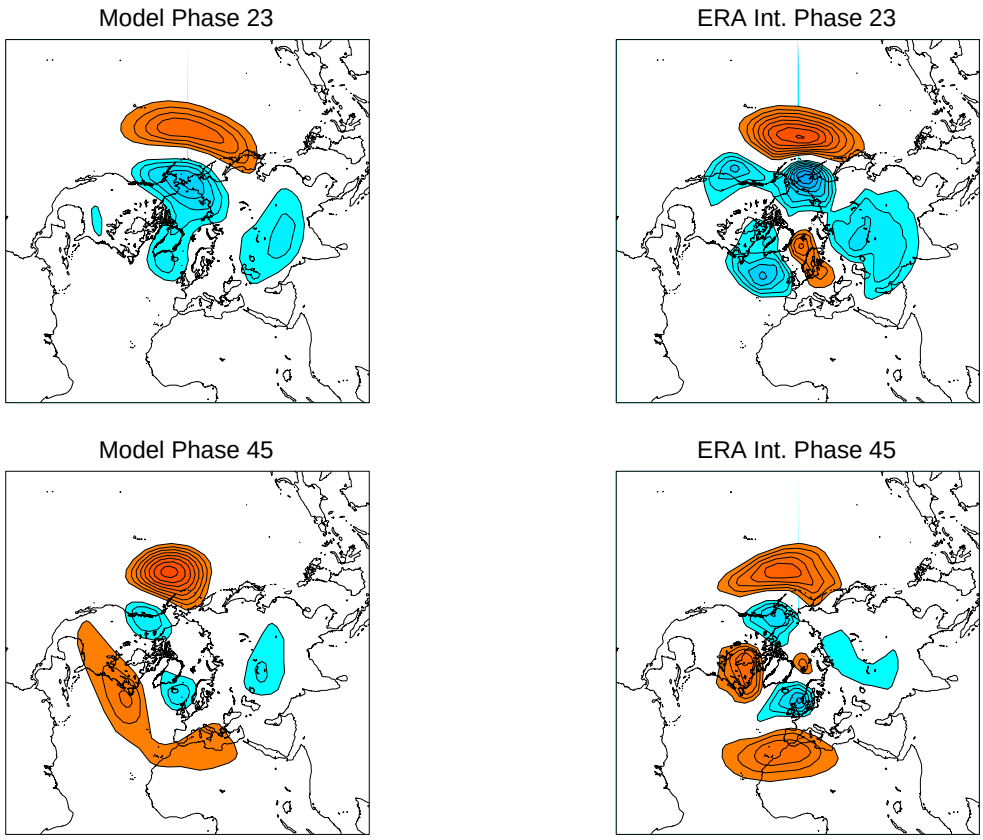

Figure 15: Phases 2+3 and 4+5 MJO composites of 500 hPa geopotential height anomaly for the day 16-45 hindcasts (left panels) and ERA Interim (right panels). Red and orange colours indicate positive anomalies. Blue colours indicate negative anomalies. The lowest contour is at 10m and the contour interval is 5 metres.

phases 2+3 and 6+7 (phases 4+5 and 8+1). Over the Euro-Atlantic sector, the impact of the MJO on 500 hPa geopotential height anomalies is generally weaker than in the reanalysis, particularly over Southern Europe.

According to Cassou (2008) the impact of the MJO in the Euro-Atlantic sector is mostly through its impact on the positive and negative phases of the North Atlantic Oscillation (NAO). The impact of the MJO on the Atlantic Ridge and Scandinavian blocking is much weaker than its impact on the NAO (see Figure 3 of Cassou, 2008). The impact of the MJO on the NAO can be detected in the time evolution of the composites of phases 3 and 6. At the initial time, the composites of phases 3 and 6 do not project on the NAO, but about 10 days later the probability of a positive phase of the NAO is strongly increased for phase 3 (phase 3 + 10 days) and the probability of a negative phase of the NAO is strongly increased for phase 6 (phase 6 + 10 days). In this section, we will focus on phase 3 + 10 days and phase 6 + 10 days to evaluate if the model can reproduce this MJO impact on the NAO.

Figure 17 shows a 10-day lagged composite of 500 hPa geopotential height anomalies in the hindcasts and in ERA Interim for phases 3 and 6. The impact over the Euro-Atlantic sector is much weaker in the

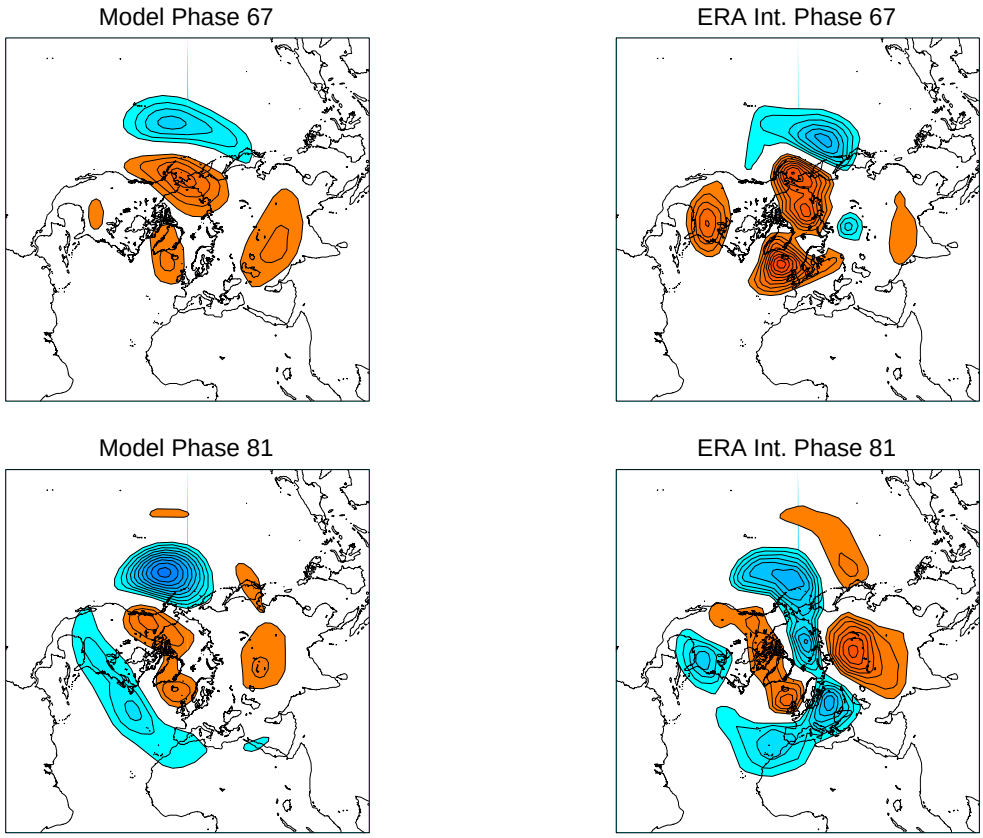

Figure 16: Same as Figure 15 but for phases 6+7 and 8+1.

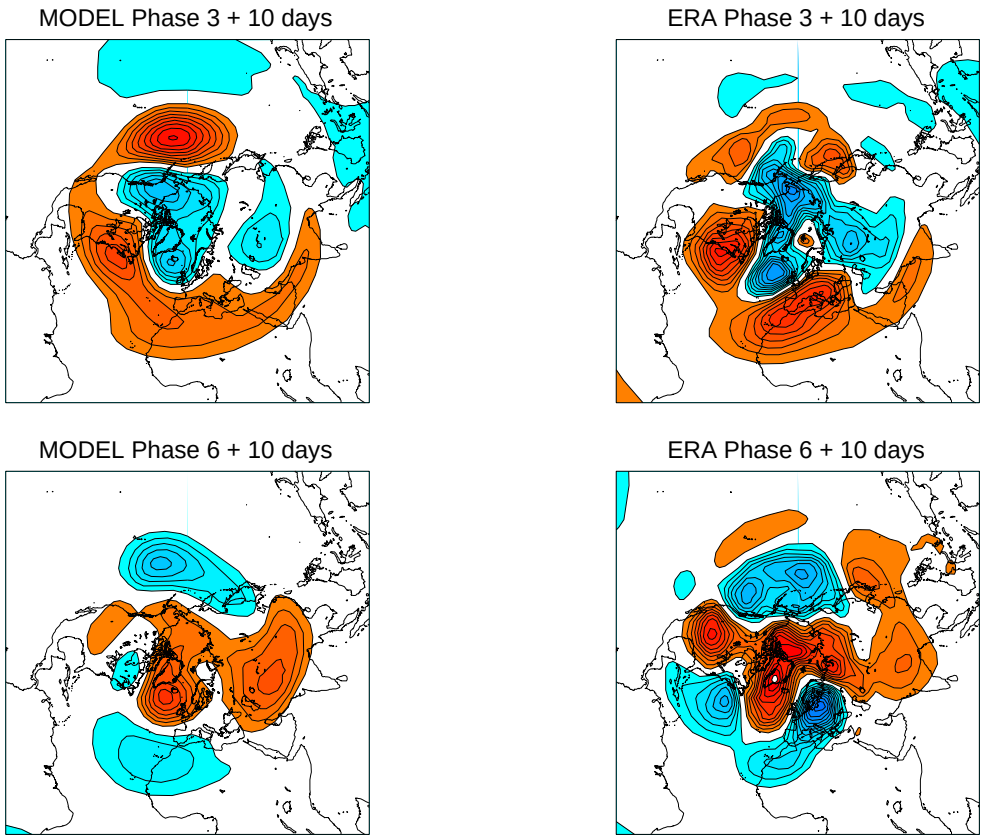

Figure 17: Phase 3 and 6 MJO 10-day lagged composites of 500 hPa geopotential height anomaly for the day 16-45 hindcasts (left panels) and ERA Interim (right panels). Red and orange colours indicate positive anomalies. Blue colours indicate negative anomalies. The lowest contour is at 5 metres and the contour interval is 5 metres.

ensemble forecasts than in the 20 years of Era Interim Reanalysis. For the 10-day lagged composite of phase 3, the amplitude of the 500 hPa geopotential height anomalies is too strong over the Pacific sector, but too weak over North-East Canada and Europe. According to Figure 18 (comparable to the left panel of Figure 4 in Cassou 2008), the propagation of geopotential height anomalies is slower and weaker in the model than in the reanalysis for phase 3. For phase 6, the wave propagation is less obvious, as mentioned in Cassou (2008), but the anomalies are also much weaker in the set of hindcasts than in reanalysis.

The fact that the MJO propagation in the model is too slow may have an impact on the MJO teleconnections. To test this hypothesis, the same composites as above have been produced for all the MJO events in phase 3 simulated by the model which have a similar propagation speed as in the reanalysis (Fig 19b: the criteria is that the MJO starting in phase 3 reaches phase 5 by day 8). Those composites are then compared to the MJO composites in phase 3 which propagate very slowly (Fig 19a: the criteria is that the MJO is still in phase 3 by day 8). The Hovmoeller diagram of 500 hPa geopotential height averaged between 40N and 60N indicates that the fast propagating model MJOs

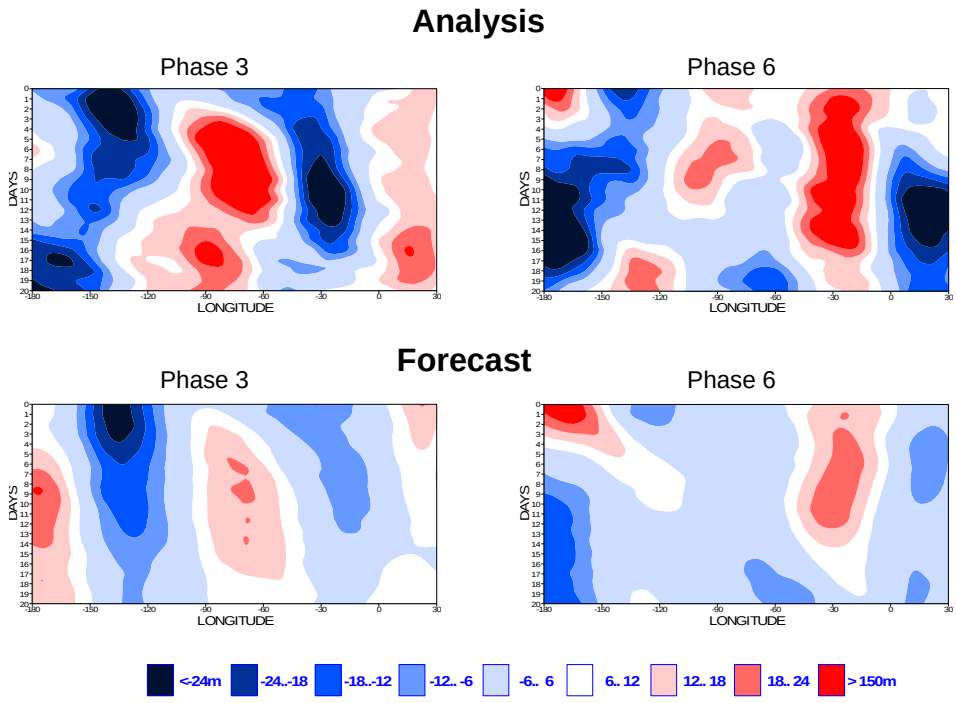

Figure 18: Hovmoeller diagram of composites of 500 hPa geopotential height anomalies averaged between 40N and 60N for phase 3 and 6 of the MJO from day 0 to day 20. The lowest contour is at 10m and the contour interval is 5 metres.

display a faster and stronger wave propagation of 500 hPa geopotential height anomalies than the slow propagating MJOs (Figs 19 c and d). The lagged composites at day 10 is shown in Figures 19 e and f for slow and fast propagating MJOs. The 500 hPa geopotential height anomaly composite obtained with the fast propagation MJOs (Fig 19f) looks more consistent with reanalysis (Fig. 17) than the composite obtained with the slow propagating MJOs (Fig 19e): over the North Pacific sector, the positive anomalies are located more to the west in the fast propagating MJO cases than in the slow MJO cases as in Reanalysis. Over North East Canada and Europe, the anomalies are significantly stronger with fast moving MJOs than with slow moving MJOs and are therefore more consistent with the reanalysis. This result suggests that some of the discrepancies between the model simulations and ERA Interim in Figure 17 are due to the fact that the MJO events in the model tend to propagate too slowly. Therefore, the current monthly forecasts over the Extratropics are likely to be negatively affected by this too slow MJO propagation in the model simulations. However even the fast propagating MJO events simulated by the model fail to produce 500 hPa height anomalies over Europe as strong as in the reanalysis and the maximum of the positive anomaly is located too much to the South, over North Africa.

The model composites are produced over the equivalent of 300 years (15 ensemble member $\times$ 20 years $\times$ 1 month period: day 16-45) whereas the reanalysis includes only 20 years. Therefore, the strong signal over Europe in the reanalysis (Fig. 17) could be due to sampling errors. To test if this is the case, the model composites have been computed for each individual ensemble member, instead of the ensemble mean. Each ensemble member represents 20 years of forecast, which is the same sampling size as the Era Interim reanalysis from 1989 to 2008. Figure 20 shows the phase 3 teleconnections after 10 days obtained with the ensemble member 13 (left panel) and ensemble member 8 (right panel). The teleconnection patterns obtained with ensemble member 13, which has a very zonal pattern, is very close to the teleconnection of the ensemble mean (left panel of Figure 17). On the other hand, ensemble member 8 displays a teleconnection pattern very close to the one obtained with the 20 years of ERA Interim, with two strong positive anomalies in the Atlantic sector, one above the North-East Canada and the second one over Europe. The anomalies over Europe have the same magnitude as in the reanalysis. The difference between the two ensemble members suggests that there are significant sampling errors when using only 20-years of data. Therefore, the differences between the teleconnections in the model ensemble and reanalysis (Fig. 17) over the Euro-Atlantic sector may be due to sampling issues in the reanalysis. 20 years of data may not be enough to evaluate the impact of the MJO over Europe. According to Figure 21, 40-years are still not enough: when combining two ensemble members to get the equivalent of 40 years of observed data, some realisations (Pert 0+1 for instance) show a maximum of positive anomaly over North Africa, when another one (Pert 2+3) shows a maximum over North-East Europe. Another realisation (Pert 13+14) has a maximum anomaly over the Atlantic, and another one (Pert 7+8) has a maximum anomaly over South-central Europe as in the 20-year ERA Interim reanalysis (Fig 17). This suggests that there is considerable uncertainty in the impact of the MJO over the European sector, even in a 40 year period, which is about the length of the analysis used in Cassou (2008). Over the Pacific sector and western Canada there is considerably less variations from one ensemble member to another.

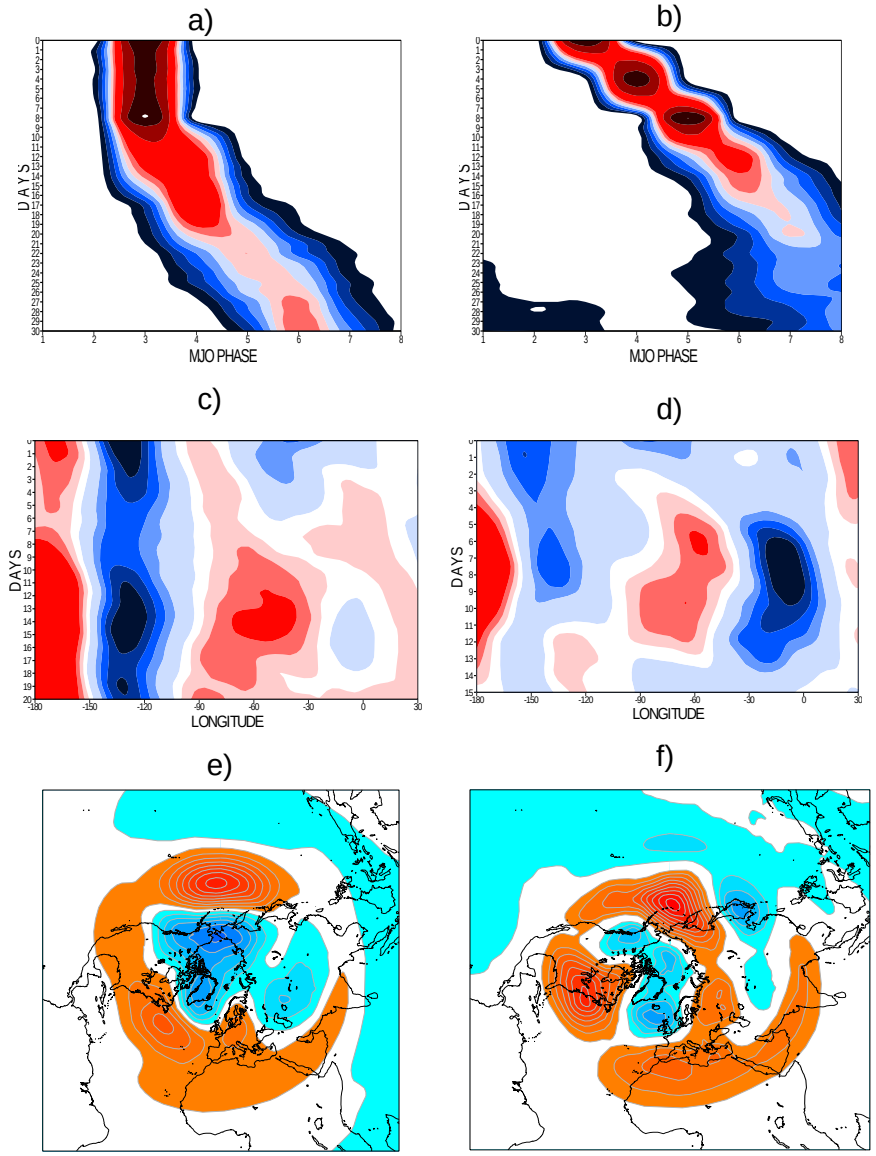

Figure 19: Hovmoeller diagram of the MJO phase as a function of lead time for the MJO events starting in phase 3 (panels a and b), Hovmoeller diagrams of composites of 500 geopotential height anomalies averaged between 40N and 60N for phase 3 of the MJO from day 0 to day 20 (panels c and d), 10-day lagged composites of 500 geopotential height anomalies (panels e and f). The lowest contour is at 10m and the contour interval is 5 metres. All the left panels correspond to MJO simulated by the model with a slow propagation. The right panels correspond to MJO simulated by the model with a fast propagation.

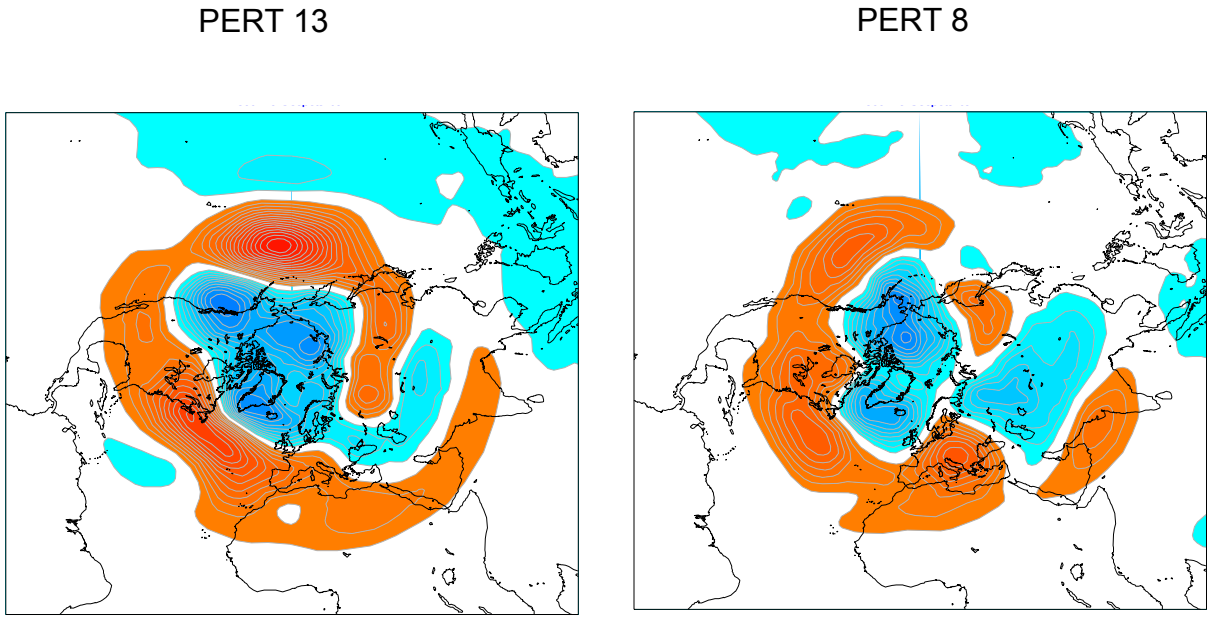

Figure 20: Same as Figure 17, but for ensemble members 8 and 13.

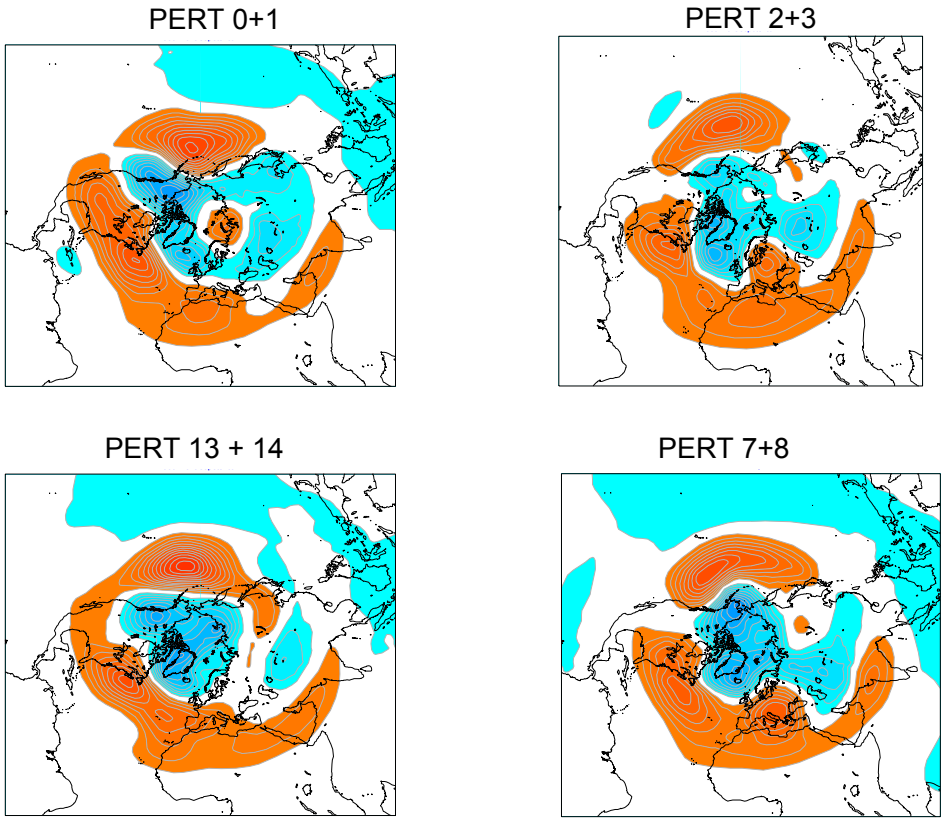

Figure 21: Same as Figure 17, but for ensemble members 0+1, 2+3, 13+14 and 7+8

4.1.2 Impact on weather regimes

Another method to investigate the impact of the MJO on the Northern Extratropics weather is to project all the forecasts or analyses associated to one specific phase of the MJO into pre-defined weather regime patterns, and evaluate if a weather regime becomes more or less likely compared to climatology. This is the method Cassou (2008) applied to a 1974-2007 analysis, and found that the MJO had a significant impact on the frequency of NAO+ and NAO- regimes,with an increased (decreased) probability of a NAO+ event 10 days after an MJO event in phase 3 (phase 6) (see Figure 3 in Cassou 2008). For NAO-, the opposite evolution takes place. In this section we project the model hindcasts and reanalysis onto 4 pre-defined weather regimes (NAO+, NAO-, Blocking, Atlantic ridge) for the period December-January-February 1989-2008. The predefined weather regimes will be described in a forthcoming technical report by S. Corti and L. Ferranti.

Figure 22 indicates that the probability of a NAO+ event increases with time during the 15 days following an MJO event in phase 3 in the majority of ensemble members. Only 4 ensemble members over 15 produce a decrease of probability of NAO+. This result is consistent with Cassou (2008) but the increased probability of a NAO+ event for the ensemble mean is only about half the increase obtained with ERA Interim (red line in Fig. 22). However the increase obtained with ERA Interim is within the spread of the 15-member ensemble, and there are a couple of ensemble members which show an evolution very close to ERA Interim. Therefore it is not clear if the discrepancy between the ensemble mean and ERA Interim is due to an inadequacy of the model to represent correctly the MJO teleconnections or if this is due to the fact that 20-year of reanalysis is too short to evaluate the impact of the MJO on weather regimes. The rigid definition of weather regimes may also contribute to the surprisingly large spread in Figure 22, since two relatively close weather patterns can be identified as different weather regimes. If we consider only the fast propagating MJO events, the probability of NAO+ events increases slightly, but still remains below ERA Interim (green curve in Fig. 22).

The probability of NAO+ diminishes in days following an MJO event in phase 6 in both ensemble mean and ERA Interim (right panel of Figure 6). For this phase of the MJO, ERA Interim and the ensemble mean are much more consistent than for phase 3. For the ensemble mean, the decrease in the probability of NAO+ has the same amplitude as the increase after phase 3. For ERA Interim, the decrease is weaker than in Figure 3 of Cassou (2008) where it reached about 40% by day 12 and is about half the amplitude of the increase from phase 3.

In the model, the impact of the MJO on the negative phase of the NAO (Fig 23) is much weaker than its impact on the positive phase of the MJO, and Figure 23 does not display a significant change in the probability of NAO-, unlike ERA Interim. The amplitudes of the NAO- variations displayed by ERA Interim are generally consistent with Cassou (2008). However, ERA Interim lies within the ensemble distribution, which is very large. A few ensemble members show a similar evolution as ERA Interim. Figure 24 shows that even if we group 2 ensemble members together to get the equivalent of 40 years of data, the spread of the ensemble remains very large and includes the change of probabilities displayed in Figure 3 of Cassou (2008)

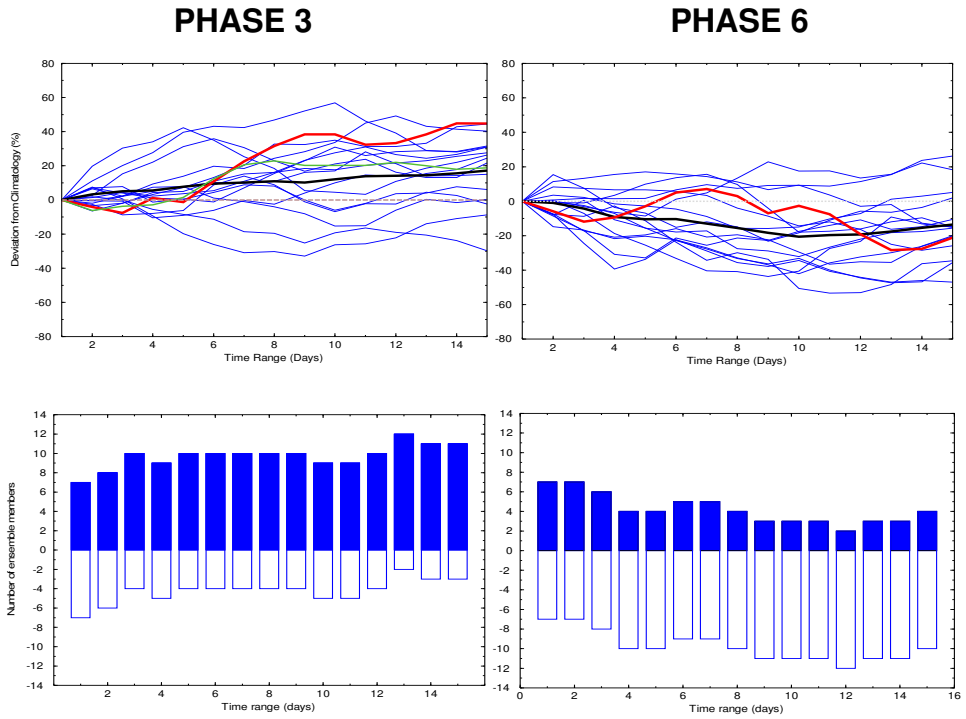

Figure 22: The top panels show the time evolution of the percentage of days in NAO+ relative to climatology as a function of lead time from phase 3 (left panel) and phase 6 (right panel). Each blue line represents an individual ensemble member. The black line represents the 15-member ensemble mean. The red line represents ERA Interim, and the green line in the top left panel represents the fast propagating MJO cases. The bottom panels show the number of ensemble members which display an increase (blue bars) and a decrease (white bars) of the frequency of NAO+ events.

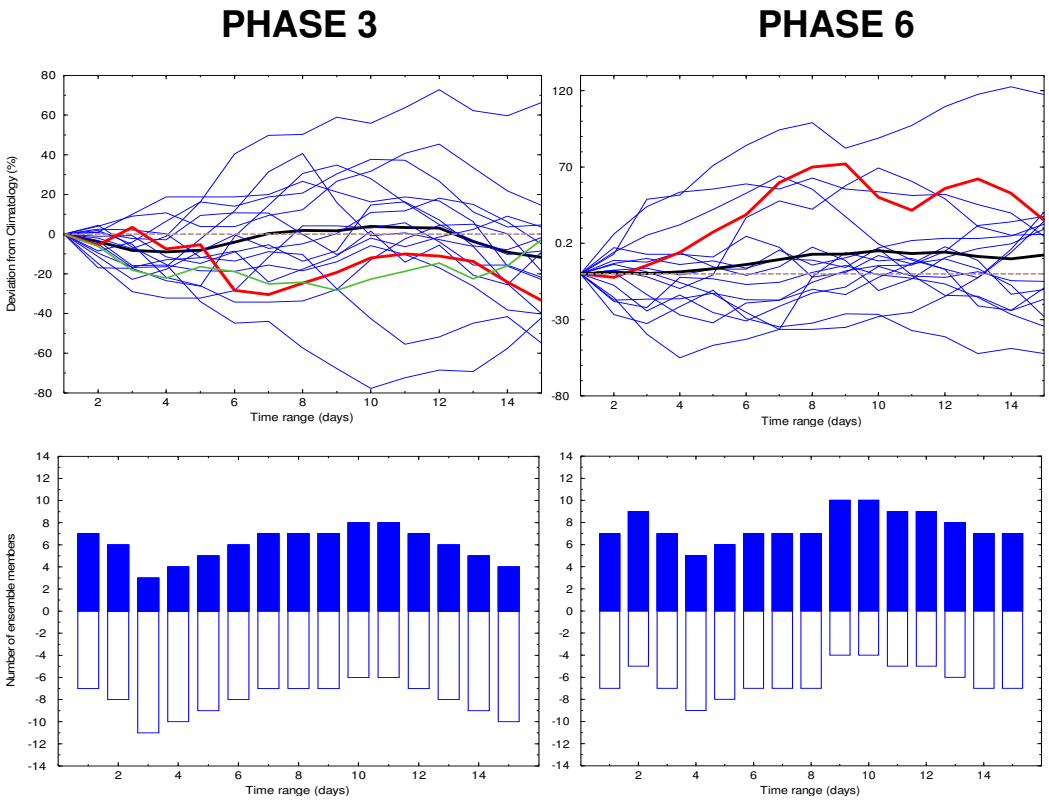

Figure 23: Same as Figure 21, but for NAO-

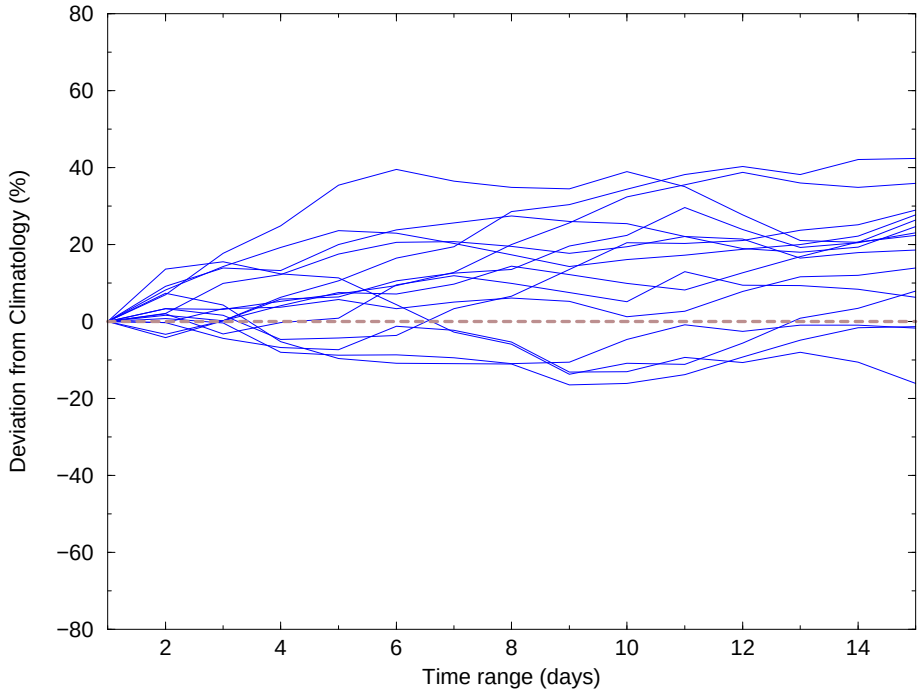

Figure 24: Time evolution of the percentage of days in NAO+ relative to climatology for 15 combinations of 2 ensemble members. The ensemble members are combined by two to get the equivalent of a 40-year reanalysis.

4.1.3 Summary

In conclusion, this section has shown that the impact of the MJO on 500 HPa geopotential height anomalies displays similar patterns to observations. However the impact over the North Pacific seems too strong compared to Era Interim and the impact on eastern Canada is generally too weak in the 10-day lagged composites from MJO phase 3. However, Figure 18 shows that those issues are partially solved when we consider only the MJO events which propagate as fast as in observations. Therefore the fact that the MJO often propagates too slowly in the model has a negative impact on the MJO teleconnections in the Extratropics.

The impact of the MJO over Europe remains unclear. The composites from the 15-member ensemble hindcasts display a much weaker impact of the MJO over Europe than 20-years of ERA Interim. The impact of the MJO over Europe is also weaker but more realistic when considering only the fast propagating MJOs. According to Figure 20, the MJO teleconnections over Europe can display considerable variability from one ensemble member to another. This is also true when grouping the ensemble members by 2 (Fig. 21) to simulate a 40-year long data. This result is confirmed when using weather regime classification. Therefore it is not clear at this stage if the model does not produce the correct MJO teleconnections over Europe, or if the strong teleconnections in ERA Interim or ERA 40 are there by chance.

This last hypothesis is reinforced by the very large spread in the ensemble distribution and by the fact that a few ensemble members can reproduce fairly accurately the very strong teleconnections produced by ERA Interim. However it could be argued that if the model MJOs had the correct speed, the teleconnections would be closer to ERA Interim and the ensemble spread may become much smaller. At this stage it is difficult to conclude one way or another.

4.2 Impact in the Tropics

In this section, the impact of the MJO on precipitation over the Tropics will be discussed. The impact of the MJO on African summer rainfall, the Indian monsoon and tropical cyclogenesis will also be discussed.

4.2.1 Impact of the MJO on precipitation

Figures 25 and 26 show the composites of total precipitation anomalies for phases 2+3, 4+5, 6+7 and 8+1 for the period November to April (Fig. 25) and June to August (Fig 26) 1989 to 2008. The eastward propagation of the MJO from one phase to another is visible over the Indian Ocean and West Pacific in both seasons, with some differences between winter and summer cases. In summer the prediction anomalies are mostly North of the Equator, whereas in winter they tend to be located more to the South. The model(right panels) represents reasonably well the main features of this eastward propagation in winter and summer.

In winter (Fig. 25), the MJO composites from ERA Interim show an impact of the MJO on precipitation over Equatorial Africa and and over Brazil. Phase 2+3 is associated with drier conditions over Brazil and Equatorial Africa, whereas phase 8+1 is conducive to wetter conditions over Brazil and

Equatorial Africa. Those teleconnections are generally well captured by the EPS hindcasts, although the anomalies over Africa tend to extend a bit more to the east than in ERA Interim. The model simulates wet conditions over South-East of the US during phase 8+1. ERA Interim displays a similar pattern but more to the North-east. Those patterns are not a trivial consequence of an MJO event because they are located east of 180E, where the eastward propagation of convection associated to the MJO stops. Therefore the model seems to capture quite well the general impact of the MJO in the Tropics in winter.

In summer (Fig 26), the MJO has a significant impact over Central America. Those teleconnections consist of wet anomalies during phase 2+3 and 8+1 and dry anomalies during phases 4+5 and 6+7. The model reproduces very well those teleconnections, which suggests that the model should have strong skill to predict precipitation in that area a few weeks in advance. Interestingly those teleconnections over Central America are very consistent with the impact of the MJO on tropical cyclone activity over Atlantic and the eastern North Pacific (Vitart, 2009). During MJO phase 2+3 and 8+1, tropical cyclone activity is enhanced over Gulf of Mexico and eastern the EPS hindcasts (Fig. 3 in Vitart 2009). Over Equatorial Africa, the impact of the MJO is limited to phase 2+3 (wet anomalies) and phase 6+7 (dry anomalies). This will be discussed in the next section.

In the model, the impact of the MJO on the Extratropics is generally much weaker than in ERA Interim. For instance the positive anomaly over China in phase 8+1 in ERA Interim during Summer is not reproduced by the model. It is however not clear how statistically significant those extratropical anomalies are.

4.2.2 Impact on African summer rainfall

The impact of the MJO during the summer season over Africa is mostly limited to MJO phases 2 and 6, which are opposite. During phase 2, ERA Interim displays a significant increase of precipitation over the Equatorial band of Africa, although the signal can be noisy (Fig. 27a). During phase 6, the impact of the MJO is the opposite to phase 2, with drier conditions over most of Equatorial Africa, although the dry anomalies do not extend to East Africa (Fig. 27b).

In the model the impact of the MJO phase 2 and phase 6 on African rainfall is generally consistent with ERA Interim (Fig. 27 a and c), although the dry anomalies extend too much to the east for phase 6 in the model. The amplitude of the impact is also weaker in the model than in observations during phase 6. The patterns in the model are not as noisy as in ERA Interim, but this is probably due to the fact that the model integrations represent the equivalent of 300 years, instead of just 20 years for ERA Interim.

4.2.3 Impact on the Indian monsoon

In this section, composites of Indian summer rainfall anomalies have been produced for the days preceeding and following an MJO event in phase 2. Figure 28 shows the evolution of those composites before and after an MJO event in ERA Interim. Five days before phase 2, dry anomalies prevail over Bay of Bengal. At day 0 (during phase 2), wet anomalies increase over the tropical Indian Ocean, and in the following pentad those wet anomalies propagate northward, to cover most of South India

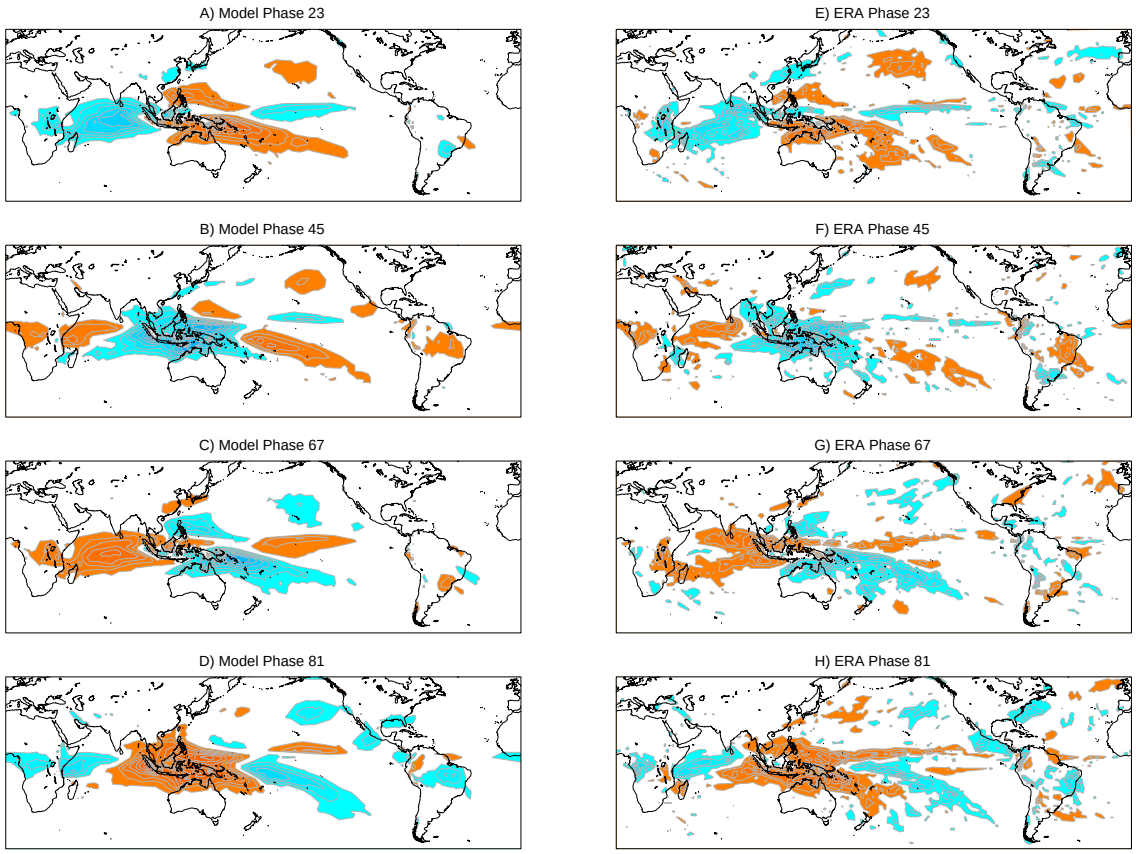

Figure 25: MJO composites of total precipitation for the day 16-45 hindcasts (left panels) and ERA Interim (right panels) for the period November to April 1989-2008. Red and orange colours indicate negative anomalies (dryer conditions). Blue colours indicate positive anomalies. The lowest contour is at 0.5 mm/day and the contour interval is 0.5 mm/day

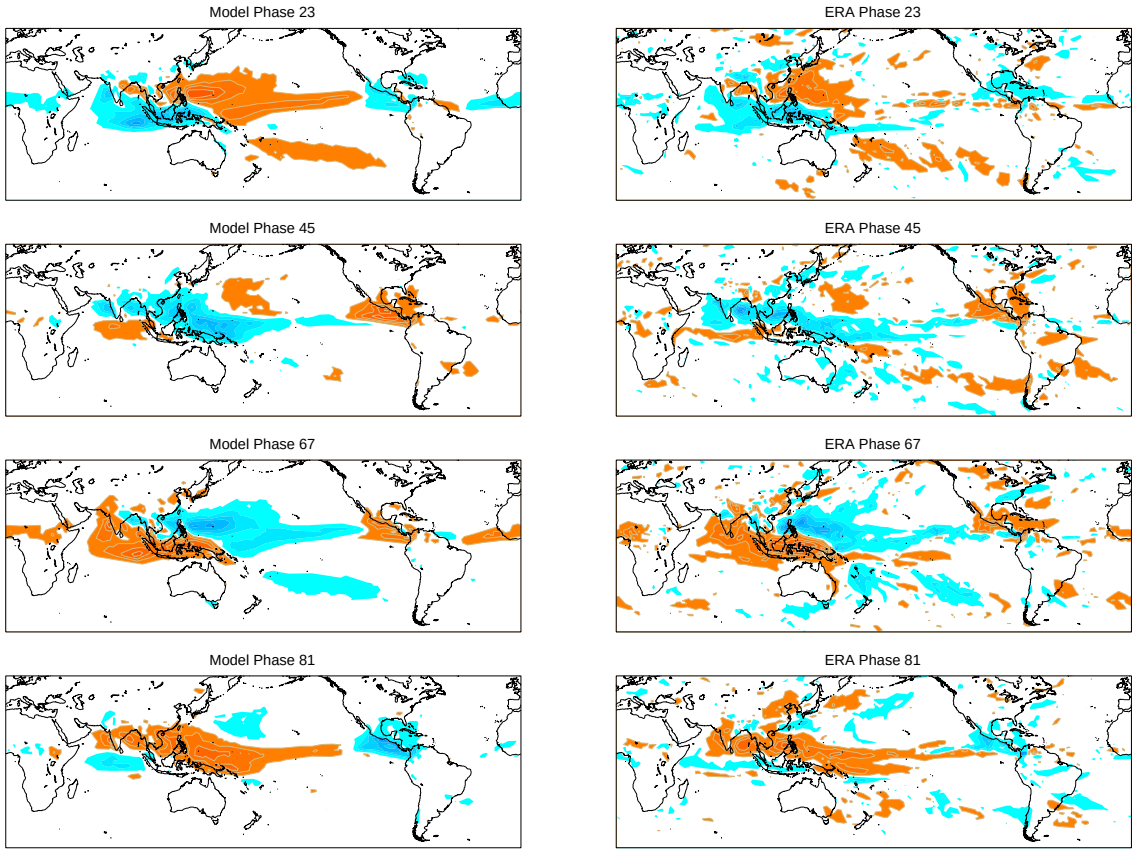

Figure 26: Same as Figure 25 but for the period June-July-August 1989-2008

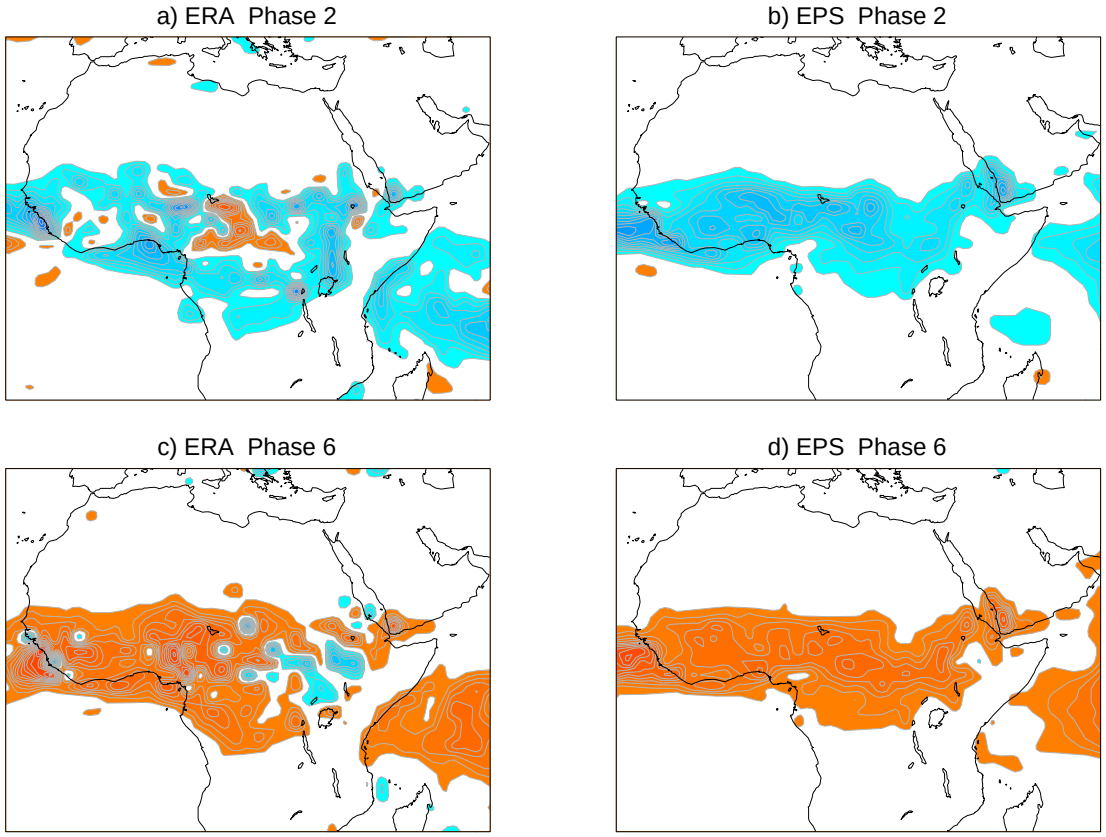

Figure 27: MJO composites of total precipitation for the day 16-45 hindcasts (left panels) and ERA Interim (right panels) for the period July to August 1989-2008. Red and orange colours indicate negative anomalies. Blue colours indicate positive anomalies. The lowest contour is at 0.2 mm/day and the contour interval is 0.2 mm/day

10 days after phase 2, North India 5 days later and then dissipate.

The model simulates a similar northward propagation of precipitation from MJO phase 2 (Fig. 29) but the speed of the northward propagation is much slower than in ERA Interim. For instance 20 days after phase 2 (Fig 29f) the model simulates wet anomalies over most of India, whereas in ERA Interim, those anomalies are much more to the North and start to dissipate. This too slow northward propagation of precipitation in the model was already noticed in Vitart and Molteni (2008) for June precipitation rainfall. In that paper it was shown that the use of an ocean mixed-layer model, which has a much finer vertical resolution in the upper ocean than the ocean model used in EPS, could help to solve this problem. To check if this is also the case for the MJO composites, the series of 46-day EPS hindcasts was reproduced but with a T159 atmospheric resolution coupled to the same ocean mixed layer model as in Woolnough et al (2007). In this new experiment, the precipitation composites display a faster northward propagation than in the EPS experiment, and the precipitation anomalies are generally more consistent with ERA Interim (Fig. 30). Figure 31 shows an Hovmoeller diagram of total precipitation anomalies averaged between 70E and 85E as a function of latitude and days after an MJO in phase 2. The northward propagation in both models and ERA Interim is well defined and is slightly faster when the atmospheric model is coupled to the KPP mixed-layer model than in the 46-day EPS integrations. In the mixed-layer experiment, the northward propagation of precipitation reaches 25N by day 20 as in the reanalysis, when it is only at 20N in the 46-day EPS integrations.

4.2.4 Impact on tropical storm genesis

The impact of the MJO on tropical cyclogenesis has been documented in numerous observational studies (see Maloney and Hartmann, 2000b for instance). Figure 32 shows that when an MJO event propagates eastward in winter, tropical cyclone genesis displays also an eastward propagation in both ERA Interim and 46-day EPS hindcasts. According to Figure 32, phase 2+3 which corresponds to the active phase of the MJO over the Indian Ocean is conducive to an increased tropical cyclogenesis over the Indian Ocean and a reduced cyclogenesis over the Australian basin and South Pacific. During phase 6+7 (suppressed phase of the MJO over the Indian Ocean), the impact on tropical storm genesis is opposite. During phase 4+5, the cyclogenesis is increased over the Australian basin and reduced over the Indian Ocean and the South Pacific. Phase 8+1 has the opposite impact. Overall the composites of tropical storm genesis in the 46-day EPS are consistent with observations, although the impact on tropical cyclogenesis is weaker in the model than in the reanalysis over the Indian Ocean.

Vitart (2009) showed that the 46-day EPS simulates although well the impact of the MJO on the tropical cyclone track density in winter and during the period August to October over the northern Hemisphere. This paper also showed that the impact of the MJO on the risk of landfall over Australia and United States is significantly affected by the MJO in the model, in agreement with the reanalysis.

4.3 Impact on the skill of the monthly forecasts

The previous section has shown that the MJO simulated by the series of EPS hindcasts generates extratropical teleconnections which are generally consistent with observations. Therefore it is expected that the model should display higher skill when there is an MJO event in the initial conditions than

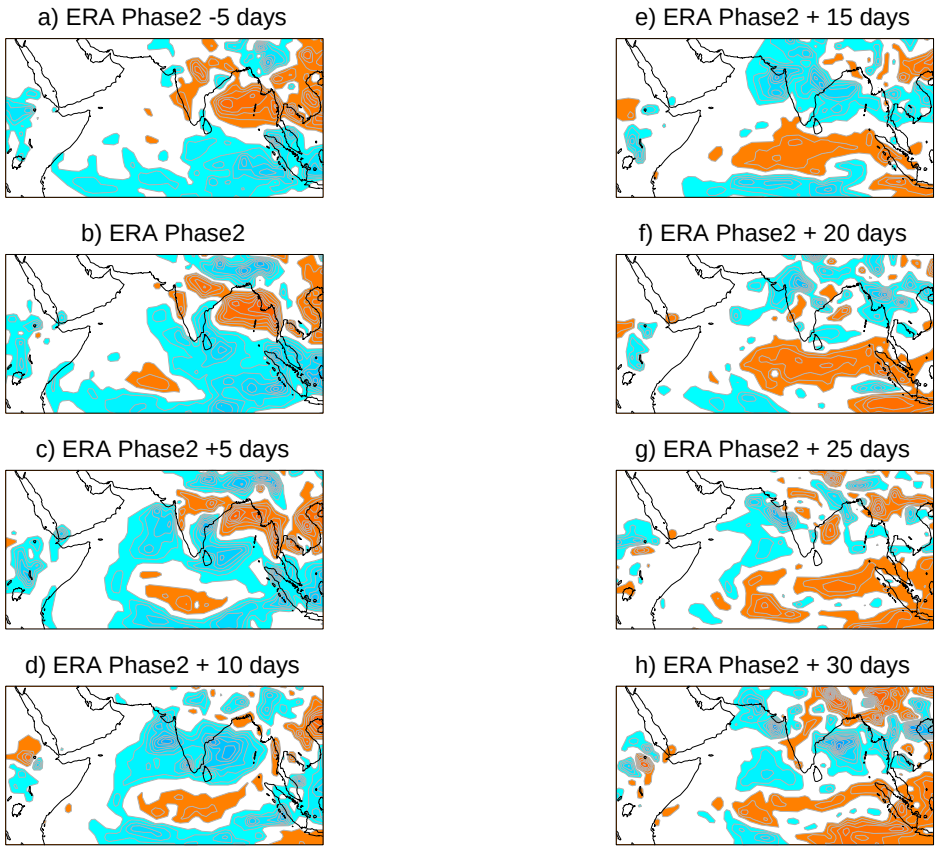

Figure 28: Lagged MJO composites of total precipitation from ERA Interim for the period June to August. Day 0 corresponds to an MJO event in phase 2. Red and orange colours indicate negative anomalies. Blue colours indicate positive anomalies. The lowest contour is at 0.5 mm/day and the contour interval is 0.5 mm/day

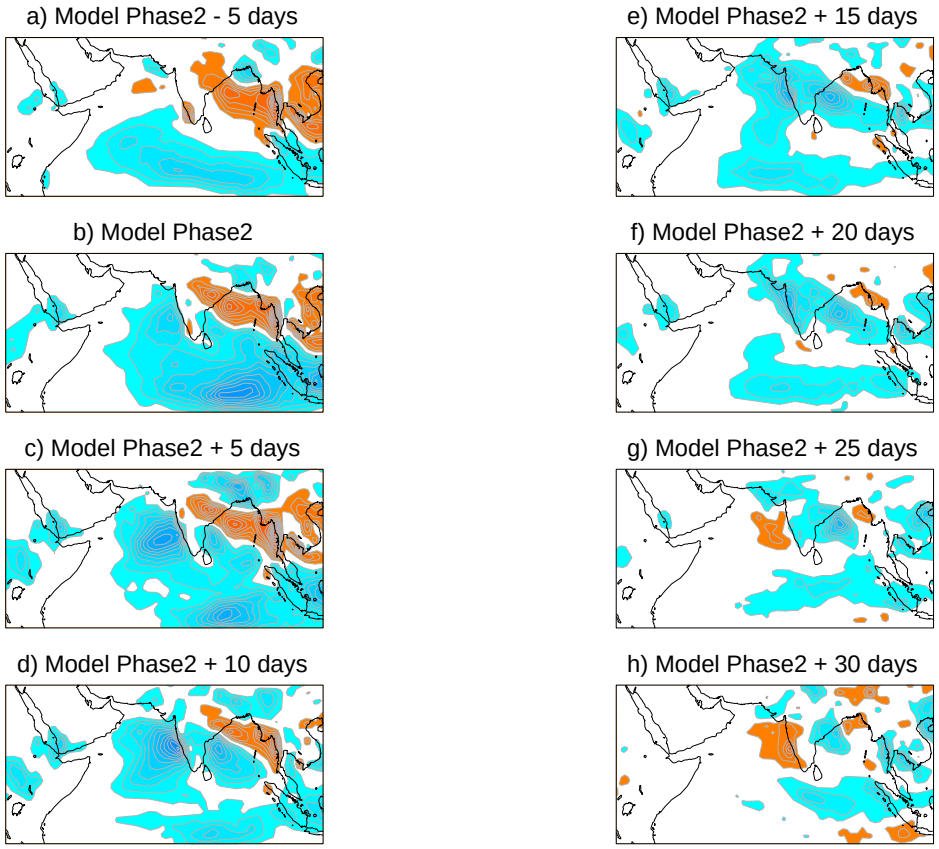

Figure 29: Same as Figure 28, but for the 46-day EPS.

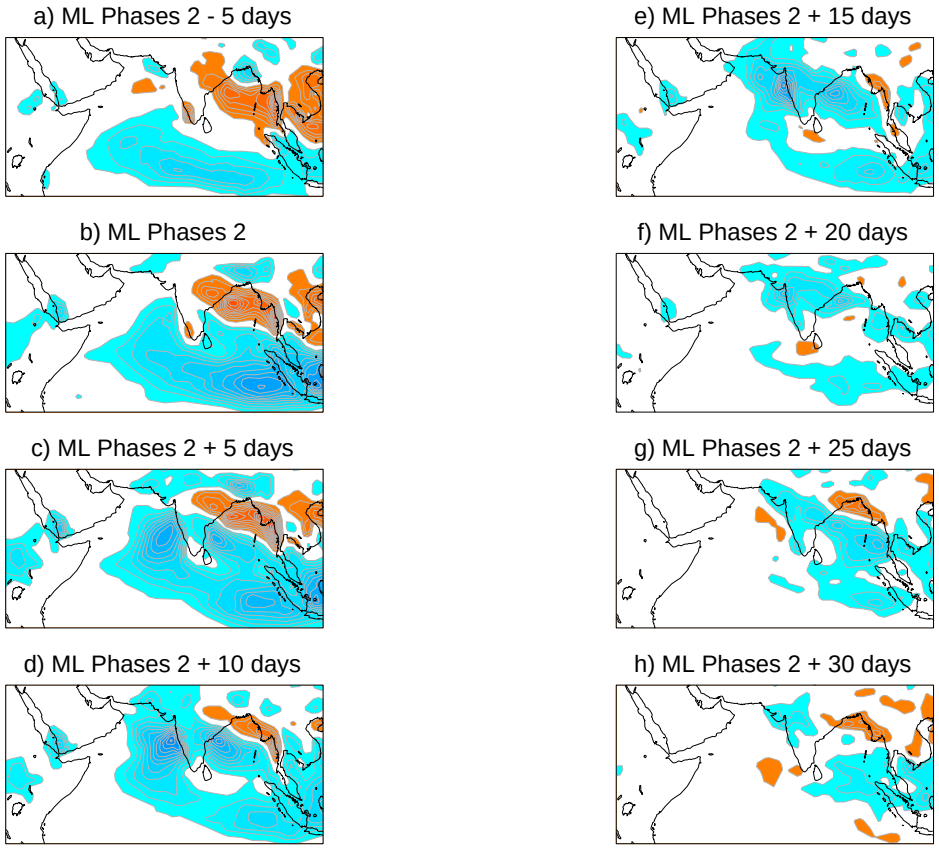

Figure 30: Same as Figure 28, but for the mixed-layer experiment.

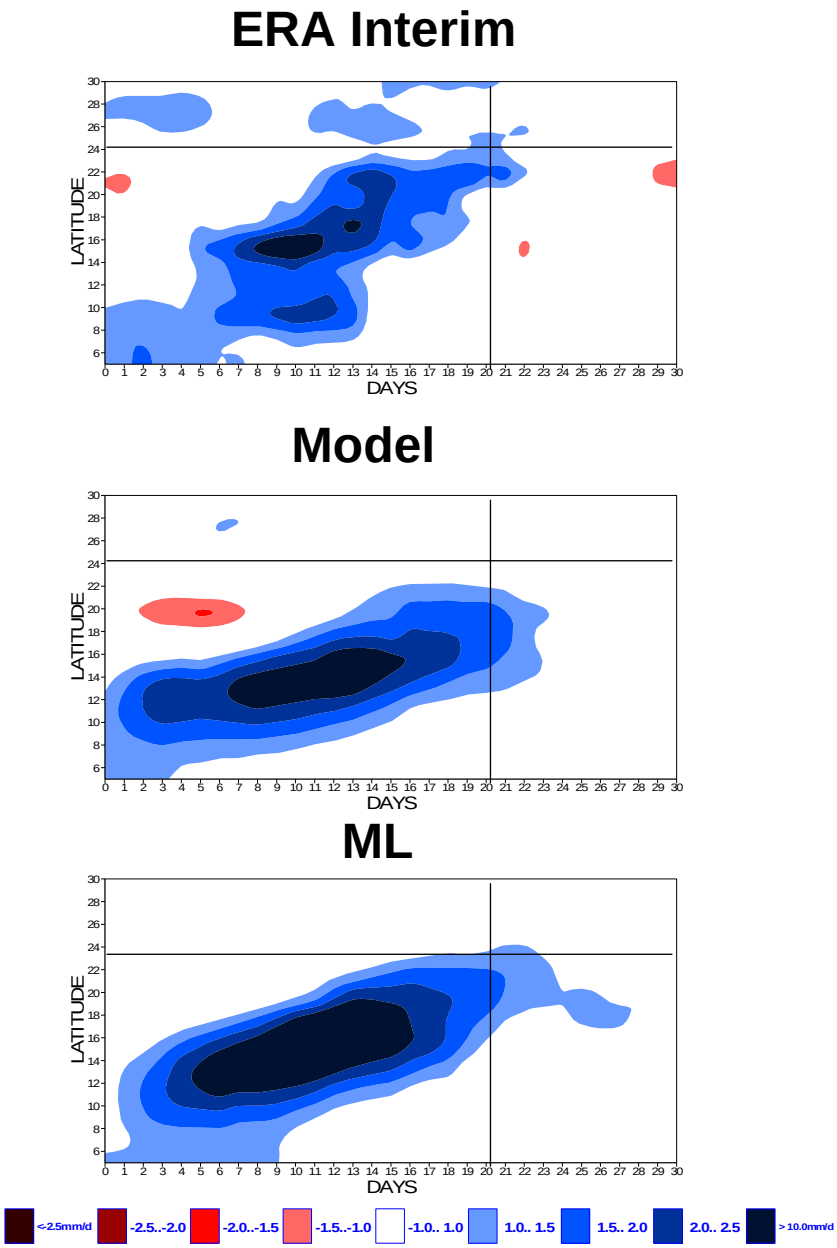

Figure 31: Hovmoeller diagram of lagged MJO composites of total precipitation averaged between 70E and 85E as a function of latitude from 5S to 30 (y-axis) and days after an an MJO event in phase 2 (x-axis) from ERA Interim (top panel), EPS (middle panel) and the experiment with a mixed-layer model (bottom panel). Red colours indicate negative anomalies (dryer conditions) and blue colours indicate positive anomalies (wetter conditions). The lowest contour is at 1 mm/day and the contour interval is 0.5 mm/day

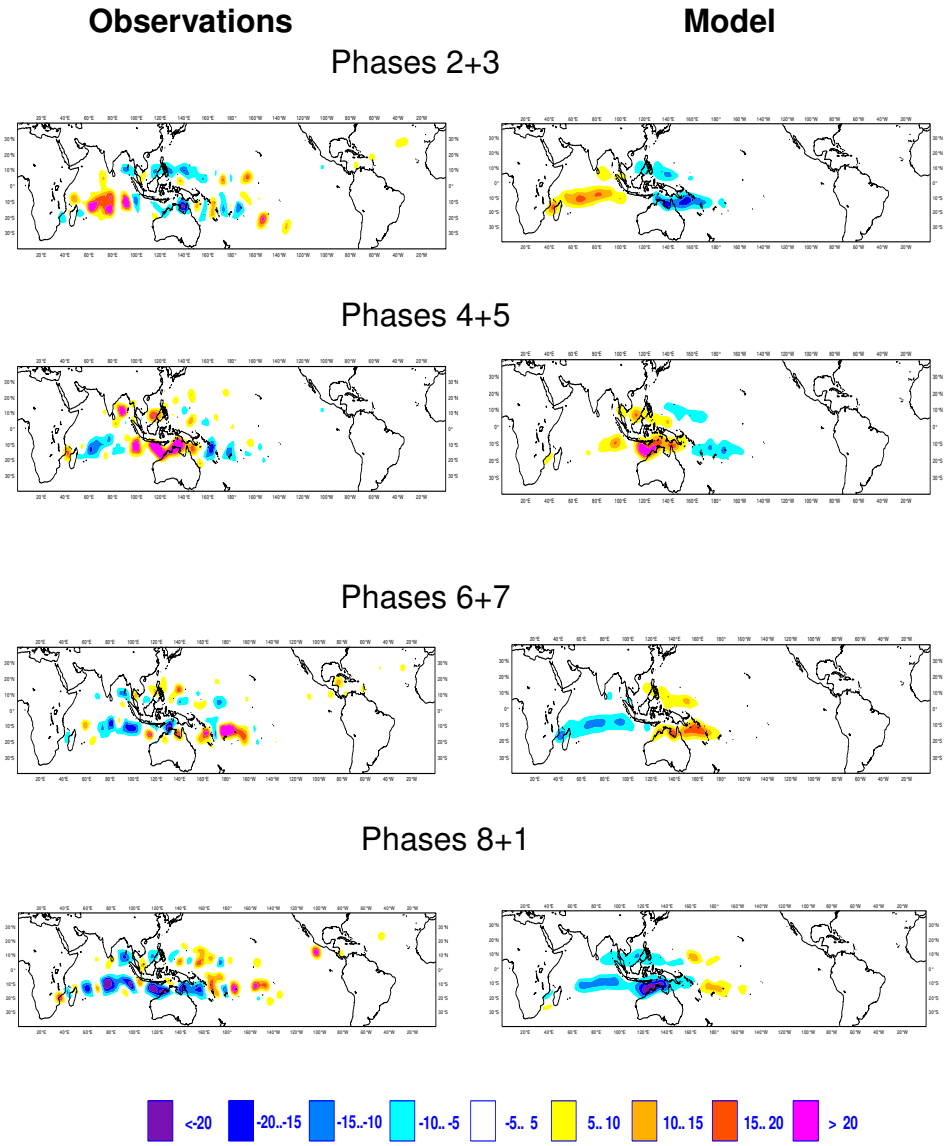

Figure 32: Tropical storm genesis density anomaly (x1000) as a function of the MJO phase in observations (left panels) and in the model hindcasts (right panels) for the period November to April 1989-2008. The anomalies are computed relative to the 1989-2008 climatology. The tropical storm genesis density is defined as the number of tropical cyclogenesis within 500 km per day. Yellow and red colours indicate an increase of tropical storm genesis. Blue colours indicate a reduction of tropical storm genesis.

when there is no-MJO in the initial conditions. Previous studies (Ferranti et al, 1990; Jones et al, 2004; Jung and Palmer 2009) have suggested an improvement of forecast skill during MJO events. Ferranti et al (1990) showed that a 20-day forecast was improved when the tropics were relaxed towards observations during an MJO event. Jones uses used a 10-year run of the NASA GCM to show that the potential predictability is increased by 2-3 days in that model. More recently, Jung and Palmer (2009) showed a reduction of extratropical forecast errors for periods wit active MJO events.

In the present paper, we use a different approach which will give us a more quantitative measure of the impact of the MJO on the monthly forecast probabilistic skill scores than the previous studies. Here we classify 120 15-member ensemble forecasts (all the forecasts starting on 15 October, November, December, January, February and March 1989-2008) as a function of the presence or not of an MJO event in the initial conditions. About 55% of the 120 cases have an MJO in the initial conditions (this MJO event can be in any phase). The ROC area and Brier skill scores have been computed for all the cases with an MJO event in the initial conditions (initial condition outside the central circle of Figure 2) for the probability that 500 hPa geopotential height, 850 hPa temperature or total precipitation are in the upper or lower tercile, for the weekly periods day 5-11, 12-18, 19-25 and 26-32 and over the northern Extratropics. For precipitation and temperature only land points have been scored. The same calculations have been repeated but this time for the case with no MJO in the initial conditions (initial conditions are in the inner circle of Figure 2).

The results for the probabilities to be in the upper tercile are displayed in Figure 33. The results are very similar for the low tercile probabilities (not shown). According to Figure 33, the ROC area and Brier skill scores are significantly higher when there is an MJO in the initial conditions (red numbers) than when there is no MJO in the initial conditions (blue numbers), except for 500 geopotential height and 850 temperature at day 5-11 where the scores are very close. The impact of the presence of an MJO in the initial conditions is particularly interesting for the period day 19-25. This time range is often considered has having very low predictability and reliability in the Extratropics (see Vitart, 2004 or Weigel et al, 2008 for instance). Therefore it is interesting to notice that when there is an MJO event in the initial conditions, the forecasts over the Northern Extratropics have a positive Brier Skill Score for 500 hPa geopotential height and 850 hPa temperature at day 19-25, indicating that those forecasts are likely to be useful. However when there no MJO in the initial conditions, the day 19-25 forecasts have very low ROC area (close to 0.5) and negative Brier skill score, indicating that those forecasts have very low skill and are not reliable. This result is confirmed by the reliability and ROC diagrams of the probability that 850 hPa temperature is in the upper tercile for various regions , including Europe (Figs. 34 and 35). Over Europe the day 19-25 probabilistic forecasts display some reliability (curve close to the diagonal) when there is an MJO in the initial conditions, but they are not reliable (almost flat curve) when there is no MJO in the initial conditions. This result suggests that at this time range the MJO represents a major, if not the main, source of predictability.This also demonstrates that the skill at this time range is not always as low as previous studies suggested and forecasts at this time range can be potentially useful over the northern Extratropics. In a practical point of view, this result also means that the users of the ECMWF monthly forecasting system could use MJO diagrams like Figure 2 (diagrams which are available to member states) to decide if the monthly forecasts of day 19-25 should be trusted or not. For day 12-18, the presence of an MJO in the initial conditions enhances the skill of the model, but the model already displays significant skill even when there is no MJO in the initial conditions. For day 16-32, the presence of an MJO in the initial conditions also improves the probabilistic skill scores, but the probabilistic scores are very low,

even with an MJO in the initial conditions.

In order to have more details on the impact of the MJO on the Extratropical skill scores, grid point maps of Brier skill score have been plotted for the various time ranges for the probability that the 500 hPa geopotential height is in the upper tercile (Figures 36-38). Although those figures are patchy and noisy, they show that the improvement in the Brier skill scores is consistent with the teleconnection patterns displayed in the previous section, with a clear improvement over Alaska, and the eastern North of Canada, which are 2 areas where MJO events have the strongest impact on 500 hPa geopotential height anomalies. Figure 39 shows that the positive impact of the presence of an MJO event in the initial conditions on 850 hPa temperature is quite obvious over the major part of the Northern Extratropics at day 19-25. Over Europe, the impact is particularly strong for South Eastern Europe, which displays high Brier skill Scores (above 0.1) when there is an MJO in the initial conditions. Over the tropics the impact of an MJO event is also significant over most regions, including Africa. for precipitation (Fig.40) the impact in the extratopics is too noisy to draw any conclusion.

It is likely that the impact of the MJO depends on the phase of the MJO in the initial conditions. To test if this is the case, the probabilistic skill scores have been computed for cases where the MJO is in phase 2+3 (convection over the Indian Ocean), phase 4+5 (MJO over the Maritime Continent), 6+7 (MJO over the west Pacific) and 8+1 (MJO over the western Hemisphere) in the initial conditions for the different weekly periods (Fig. 41). According to Figure 41, the extratropical scores do not depend significantly on the phase of the MJO for day 5-11 and day 12-18. However, for longer time ranges (day 19-25 and 26-32) the probabilistic scores are significantly higher during phase 2+3 and 4+5 than in the other phases. This is not unexpected, since when the initial conditions include an MJO in the west Pacific or in the western Hemisphere, this MJO is likely to have disappeared by day 20 in most cases, because those MJO phases represent the end of the MJO cycle. However when there is an MJO in the Indian Ocean in the initial conditions, the MJO event is more likely to survive 3 weeks in the model.

5 Hindcasts with cycle 35R3

The result presented so far were obtained with cycle 32r3, which was operational from November 2007 until June 2008. Since June 2008, several versions of IFS have been operational. In order to see if the results presented in this paper are still relevant with the most recent versions of IFS, the hindcast integrations have been repeated for the following starting dates: 15 November, 15 December, 15 January and 15 February 1989 to 2008, with IFS cycle 35R3, which is operational from 8 September 2009. It is the most recent version of IFS at the time this report has been written.

5.1 MJO in cycle 35r3

The hindcast integrations with cycle 35r3 display better skill to predict the evolution of the MJO than the hindcasts produced with cycle 32r3 (Fig. 42). The gain of predictability is modest in the medium-range, but is of about 2 days in the extended range, with the 0.6 correlation reached around day 21, and the 0.5 correlation reached at day 26. A separate set of experiments has shown that most

a) Z500

	Day 5-11	Day 12-18	Day 19-25	Day 26-32
ROC score	0.88 0.87	0.72 0.68	0.61 0.55	0.56 0.53
Brier skill score	0.41 0.41	0.14 0.07	0.02 -0.07	-0.05 -0.06

b) T850

	Day 5-11	Day 12-18	Day 19-25	Day 26-32
ROC score	0.87 0.87	0.70 0.68	0.64 0.56	0.57 0.52
Brier skill score	0.42 0.42	0.10 0.07	0.04 -0.06	-0.02 -0.08

c) Total Precipitation

	Day 5-11	Day 12-18	Day 19-25	Day 26-32
ROC score	0.72 0.70	0.61 0.58	0.55 0.52	0.53 0.51
Brier skill score	0.12 0.08	0.01 -0.02	-0.04 -0.07	-0.06 -0.06

Figure 33: ROC and Brier skill scores for the periods day 5-11, 12-18, 19-25 and 26-32 for the probability that 500 hPa geopotential height (top panel), Temperature at 850 hPa (middle panel) and total precipitation (bottom panel) are in the upper tercile. The red (blue) numbers indicate the scores obtained when there an MJO (no MJO) in the initial conditions.

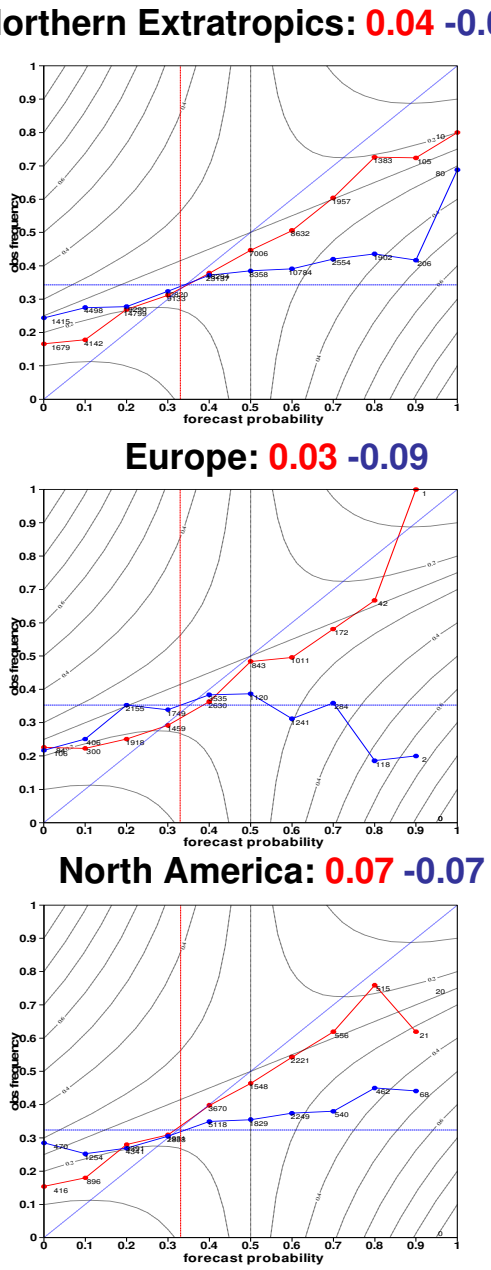

Figure 34: reliability diagram of the probability that the 850 hPa temperature is in the upper tercile for the period day 19-25 for a) the Northern Extratropics, b) Europe and c) North America. The red (blue) line represents the reliability diagram obtained with all the cases with an MJO (no MJO) in the initial conditions. The numbers represent the Brier Skill Score. Only land points have been included in the calculation of the reliability diagram and the Brier skill scores.

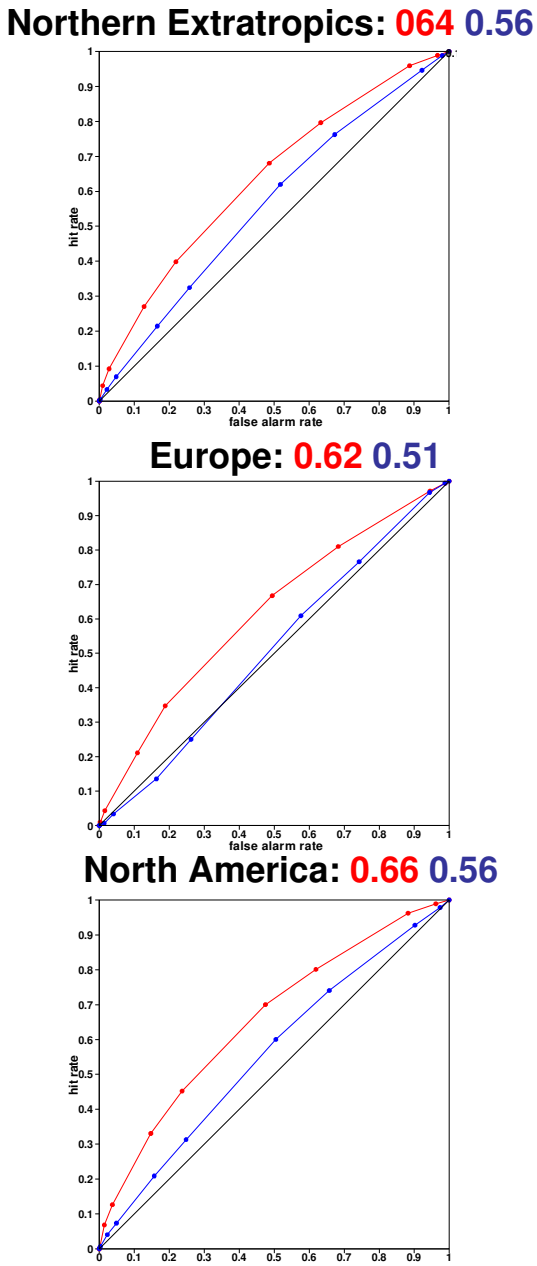

Figure 35: Same as Figure 34, but for the ROC area.

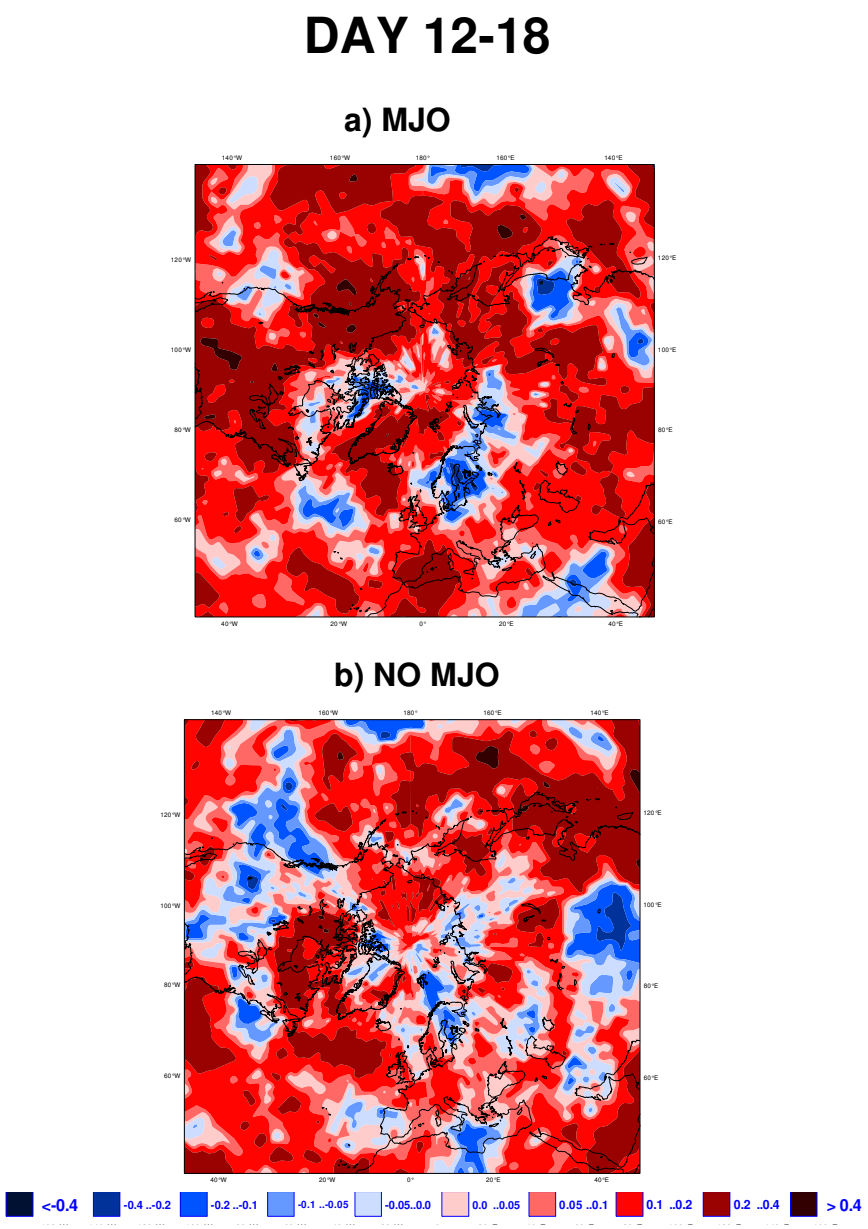

Figure 36: Brier skill score of the probability that the 500hPa geopotential height is in the upper tercile for the period day 12-18 and for the cases a) with an MJO in the initial conditions (top panel) and b) without an MJO in the initial conditions.

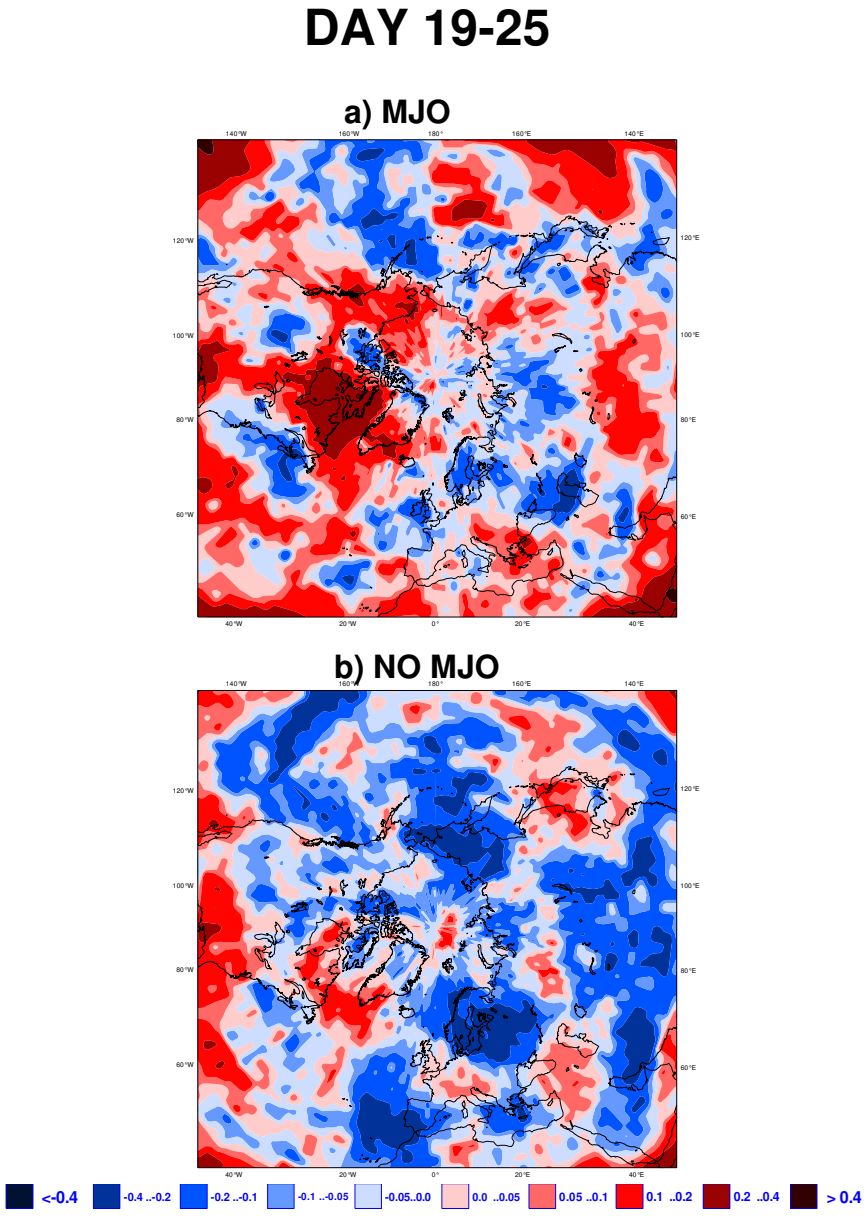

Figure 37: Same as Figure 36, but for period day 19-15.

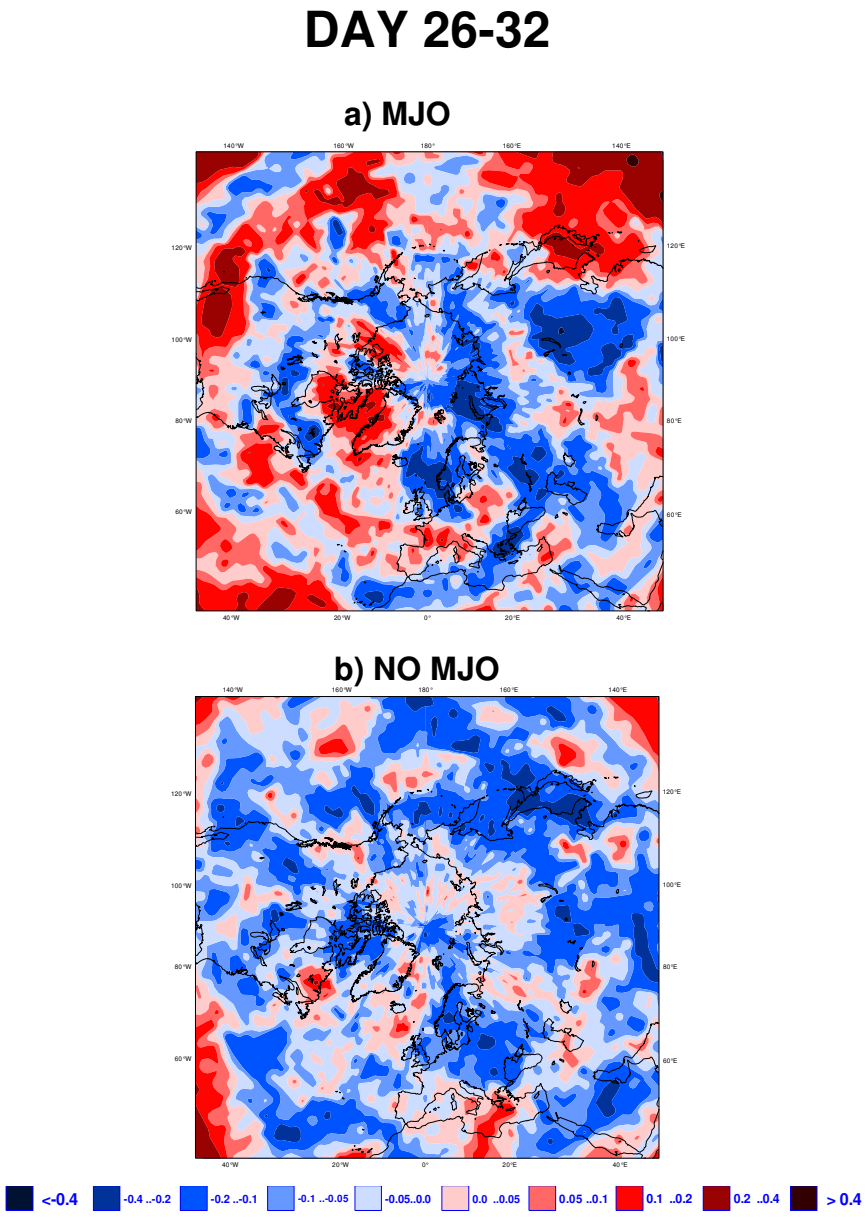

Figure 38: Same as Figure 36, but for period day 26-32.

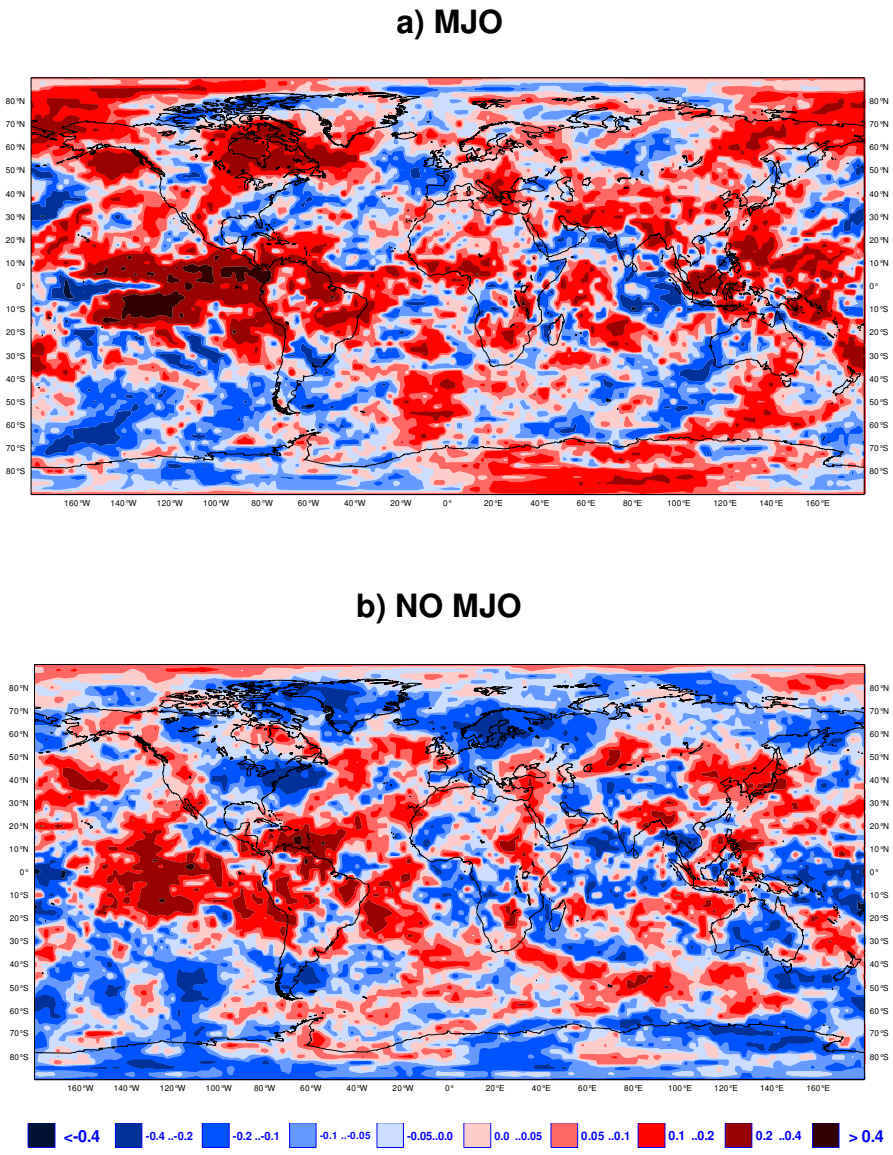

Figure 39: Same as Figure 36, but for 850 hPa temperature and the period day 19-25.

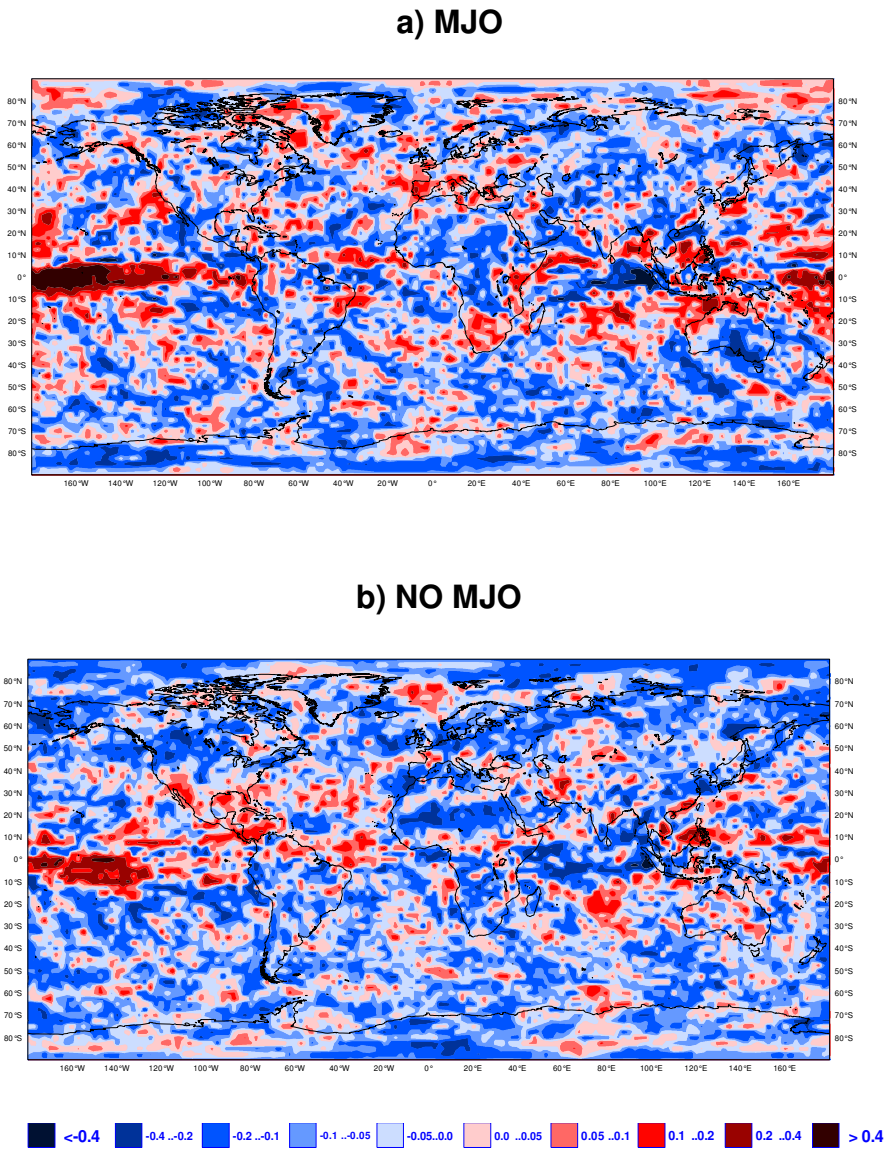

Figure 40: Same as Figure 36, but for total precipitation and the period day 19-25.

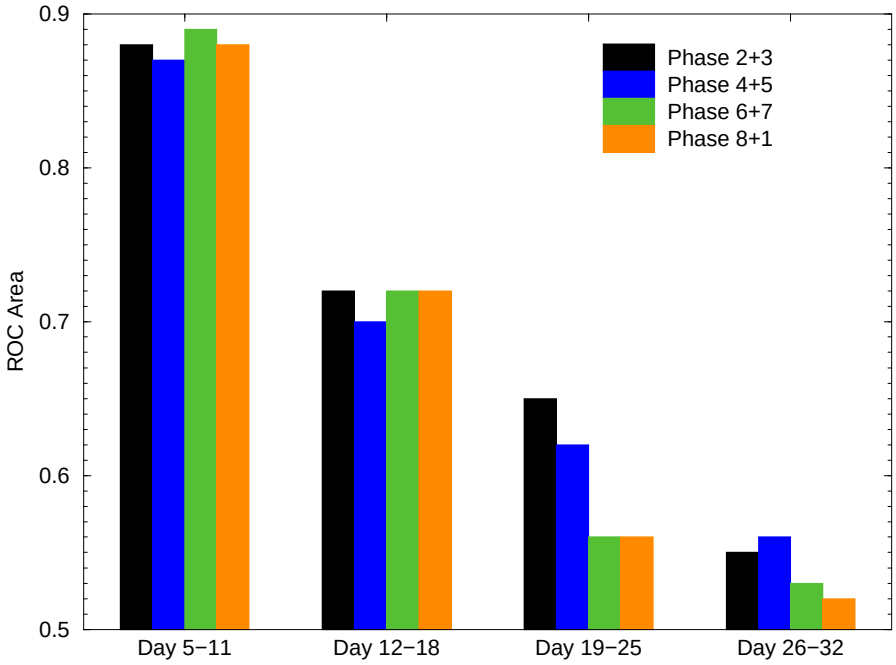

Figure 41: ROC area of the probability that the 500 hPa geopotential height is in the upper tercile for all the cases with an MJO event in phase 2+3 (black bars), 4+5 (blue bars), 6+7 (green bars) and 8+1 (orange bars) for the periods day 5-11, 12-18, 19-25 and 26-32.

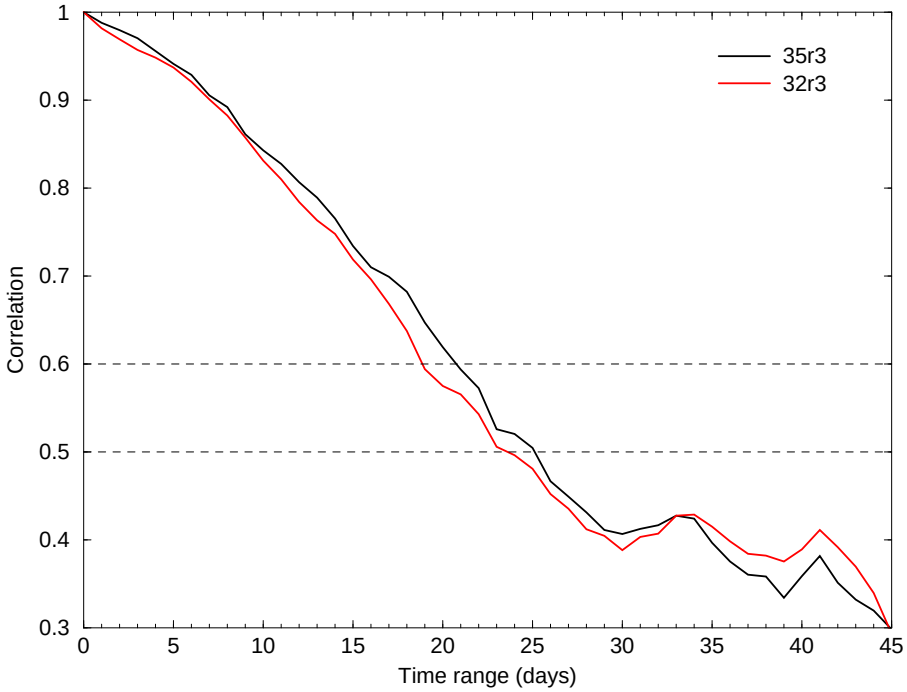

Figure 42: Evolution of the correlation between the ensemble mean of (pc1+pc2)/2 and ERA Interim as a function of the forecast lead time. The black line represents the score obtained with cycle 35R3, and the red line represents the scores obtained with cycle 32R3. All the 15-member ensemble forecasts starting on 15 November, December, January and February 1989 to 2008 have been included in the computation of the correlation.

of this improvement in MJO skill between cycle 32r3 and 35r3 comes from the introduction of the representation of the SST diurnal cycle in sunny, low wind regimes. Cycle 32r3 was overactive, and Figure 9 showed that the amplitude of the MJO was about 20% too strong after 10 days of integrations. Cycle 35r3 is still overactive with a stronger mean amplitude of the MJO after 10 days compared to ERA Interim. However, the amplitude of this bias is significantly lower than with 32R3 (Fig. 43). With Cycle 35R3, the MJO tends to be 10% too strong, which means a reduction by a factor 2 of the bias obtained with cycle 32r3. Figure 44 shows that the propagation of the MJO is still too slow compared to ERA Interim (left panel of Figure 12).

5.2 MJO teleconnections in cycle 35r3

Figures 45 and 46 show composites of 500 hPa geopotential anomalies when there is an MJO event in phase 2+3, 4+5, 6+7 and 8+1 with cycle 32r3 and cycle 35r3. The composites look very consistent between the two model cycles. The 10-day lagged composites of 500 hPa geopotential anomalies

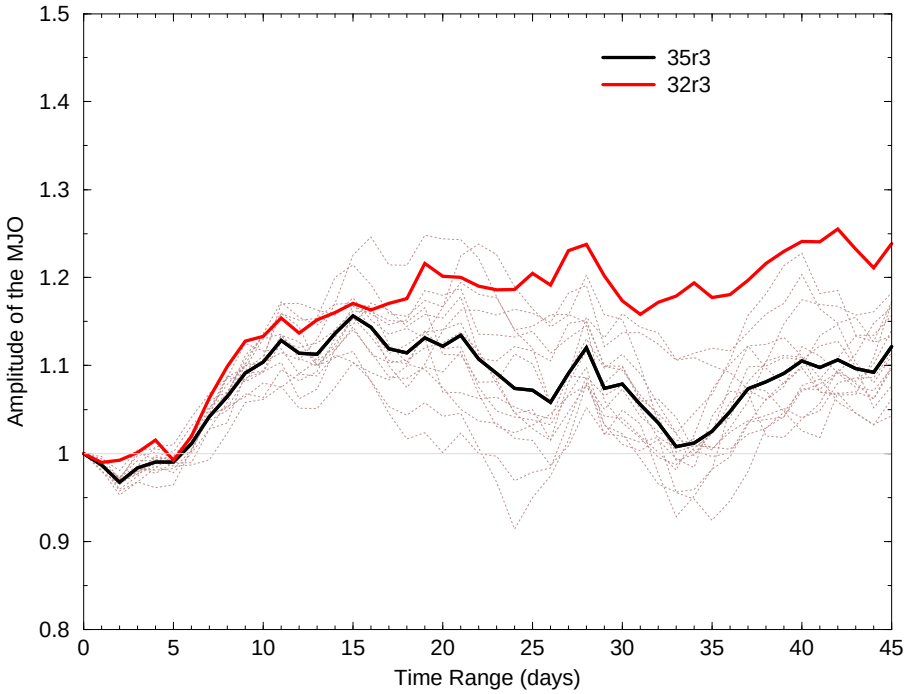

Figure 43: Evolution of the amplitude of (PC1+PC2)/2 as a function of forecast lead time (days) for the period November to February 1989 to 2008. The dotted line represents the amplitude of (PC1+PC2)/2 of individual ensemble members. The solid black (red) line represents the mean amplitude averaged over the 15 ensemble members with cycle 35r3 (32R3).

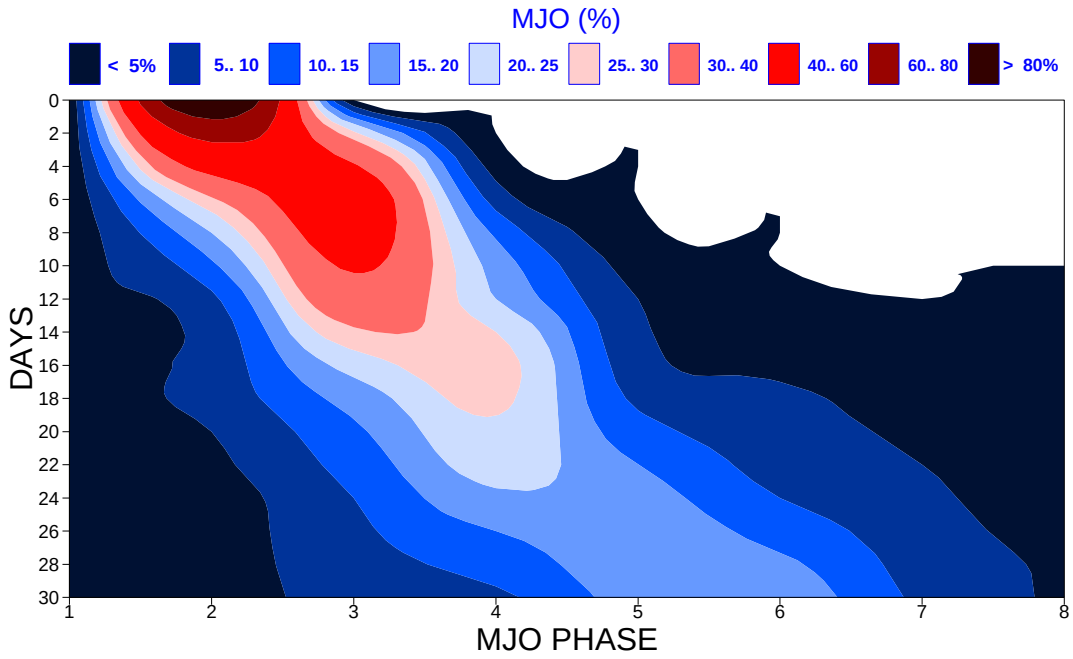

Figure 44: Same as Figure 12 but for cycle 35r3 and the period November to February 1989-2008.

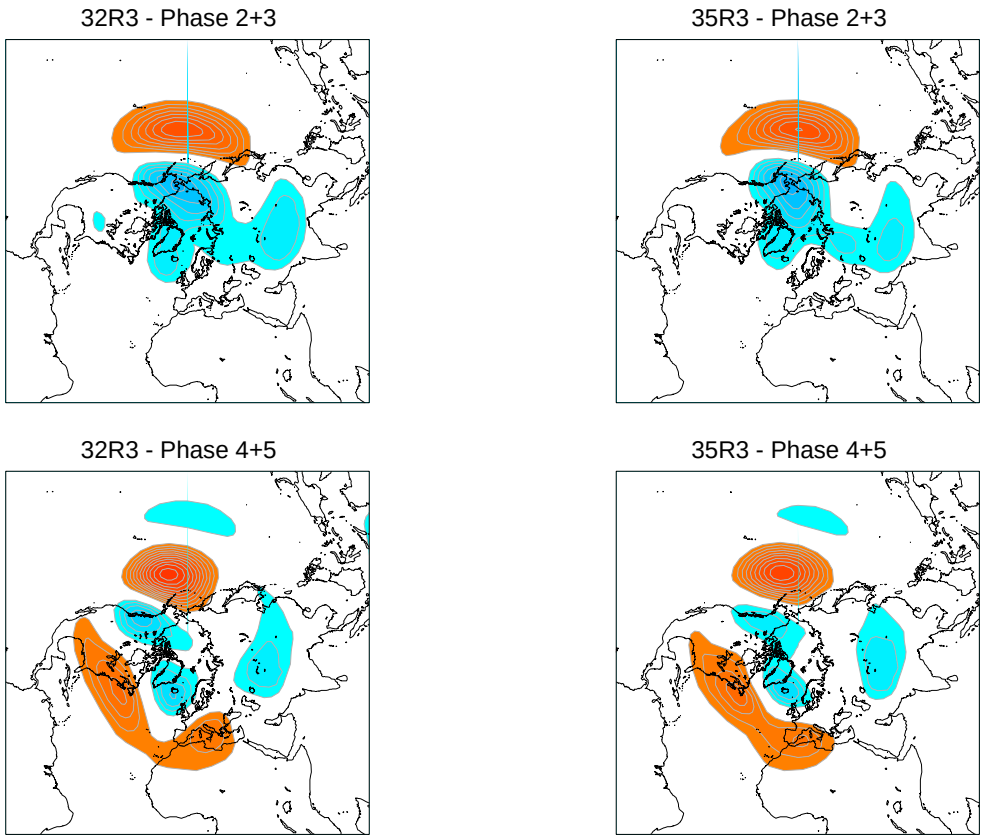

Figure 45: Composites of 500 hPa geopotential height anomaly for the day 16-45 hindcasts with Cy32r3 (left) and Cy35r3 (right panels) in MJO phases 2+3 and 4+5. Red and orange colours indicate positive anomalies. Blue colours indicate negative anomalies. The lowest contour is at 10 metres and the contour interval is 5 metres.

when there is an MJO in phase 3 (Fig. 47) are also remarkably similar between the two model cycles. Since no major change in the parameterisation of convection has been introduced between cycles 32r3 and 35r3, which could potentially affect the MJO teleconnections, this result is not unexpected. In fact it confirms that the experimental setup (the equivalent of 300 winters) is robust enough that the sampling errors are minimal. As shown in previous chapters, this would not have been the case if the ensemble size had been much smaller. It is interesting to notice that the amplitude of the MJO teleconnections are very similar between the two set of hindcasts, and this despite the fact that cycle 35r3 has an MJO mean amplitude about 10% weaker than cycle 32r3.

6 Conclusion

This paper has shown the main characteristics and impact of the MJO in a set of 15-member ensemble hindcasts. Although the model displays some skill to predict the evolution of the MJO (about 20 days

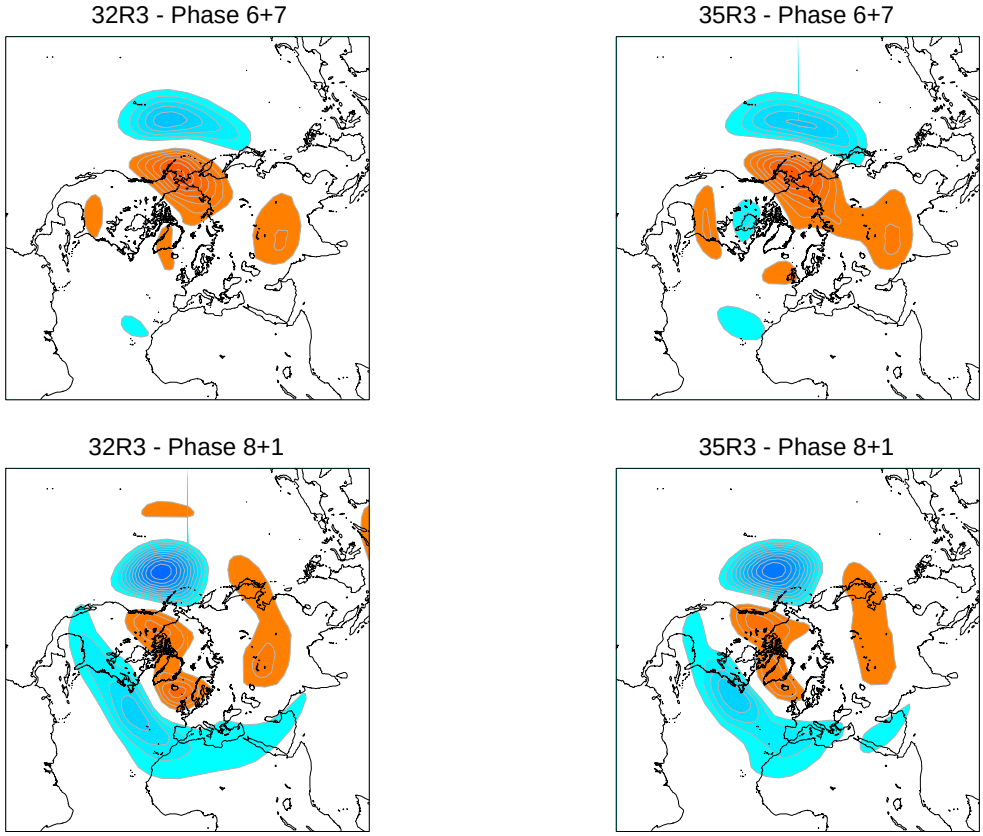

Figure 46: Composites of 500 hPa geopotential height anomaly for the day 16-45 hindcasts with cycle 32r3 (left panels) and cycle 35r3 (right panels) in MJO phases 6+7 and 8+1. Red and orange colours indicate positive anomalies. Blue colours indicate negative anomalies. The lowest contour is at 10 metres and the contour interval is 5 metres.

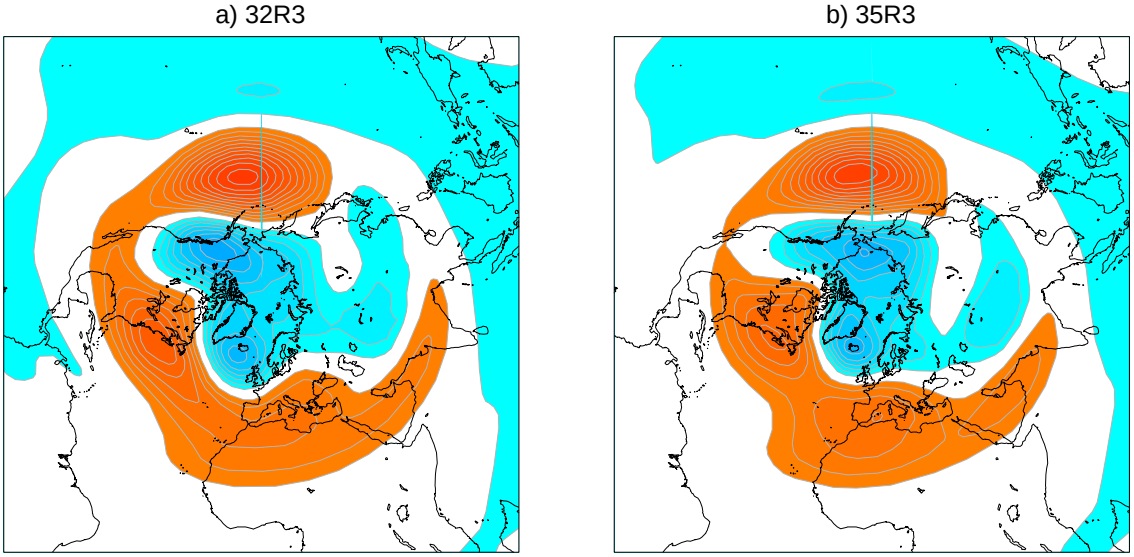

Figure 47: MJO phase 3 10-day lagged composites of 500 hPa geopotential height anomaly for the day 16-45 hindcasts with cycle 32r3 (left) and cycle 35r3 (right panels). Red and orange colours indicate positive anomalies. Blue colours indicate negative anomalies. The lowest contour is at 5 metres and the contour interval is 5 metres.

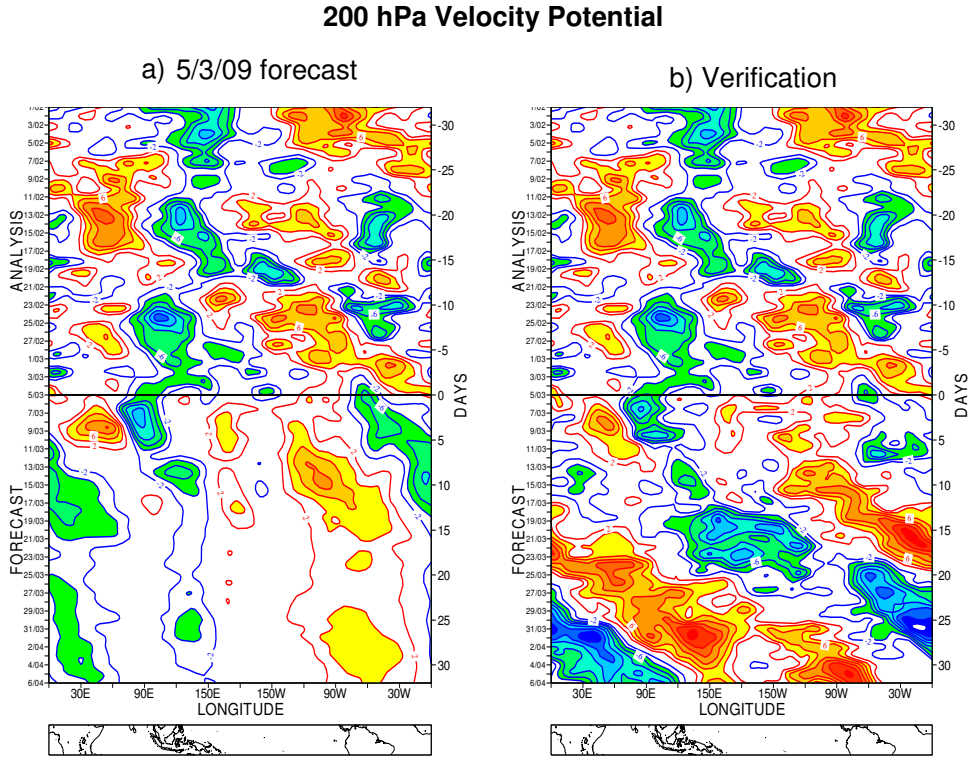

Figure 48: Hovmoeller diagram of velocity potential anomalies at 200hPa for a) the forecast starting on 5 March 2009 and b) ECMWF analysis. The top half of the plot shows the analysis of the preceeding month. The green colours indicate negative anomalies of velocity potential (positive phase of the MJO). The orange colours indicate positive anomalies (negative phase of the MJO).

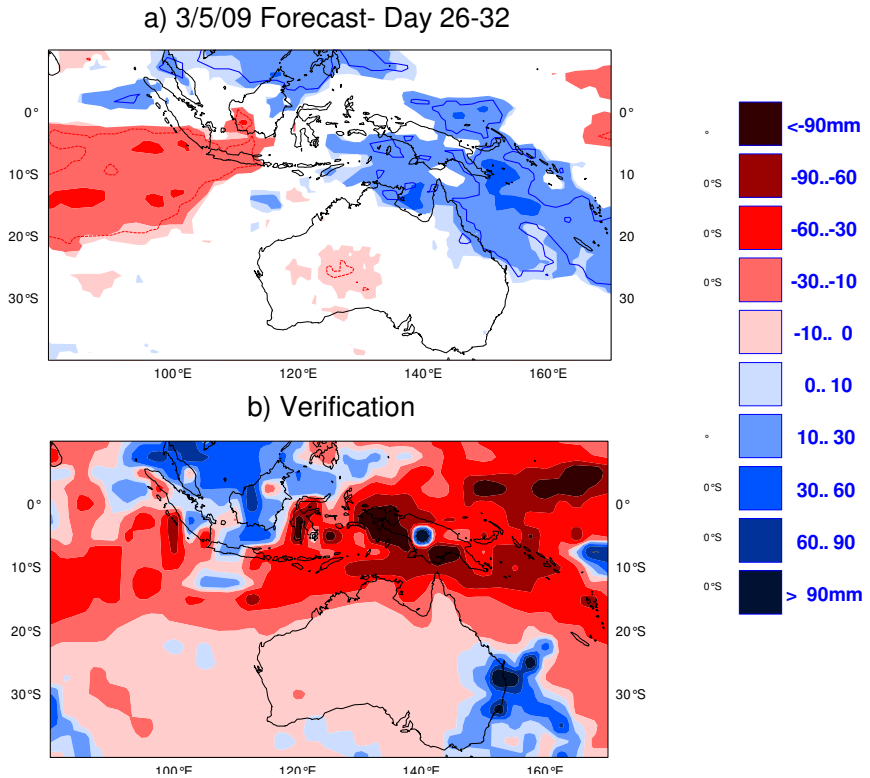

Figure 49: Precipitation anomalies for weekly period from 30 March until 5 April 2009. The left panel shows the operational monthly forecast issued on 5 March 2009 (time range is day 26 to 32). The right panel shows the precipitation anomaly computed from the ECMWF operational analysis and ERA 40.

of predictability), the MJO in this set of hindcasts has some issues:

- The MJO tends to be too strong, but this problem has been partially solved in the following model cycles (see Figure 43).

- The MJO tends to be too slow. This is not true for all the MJO simulated by the model. Figure 2 and 19 show that MJOs in the model can propagate at the correct speed, but Figures 12 shows that statistically most model MJO events starting in phase 2 reach phase 4 by day 14, which is about 4 days later than in observations. Figure 13 confirms that the model MJO events spend too much time in each MJO phase.

- The MJOs in the model have often difficulties to cross the Maritime continent (Fig. 14). Once again this is not a systematic problem. Some model MJOs cross the Maritime continent, but statistically the percentage of MJOs which do not cross the Maritime continent is significantly higher in the model than in observations. In those cases, the convections can be locked over the Maritime continent until the end of the forecast.

- The MJO teleconnections over Europe may be too weak compared to ERA Interim. It is however not clear how representative the 20-year ERA Interim teleconnections are. As shown in Section 4.1, 20 or 40 years of reanalysis are not enough to assess the impact of the MJO over Europe.

Of all those problems, the too slow propagation of the MJO is probably the most serious issue for the ECMWF monthly forecasting system, particularly for the longer time range (day 19-25 and 26-32). This too slow propagation and the difficulty to cross the maritime continent may cause the forecast to be completely out of phase with observations after 20 days. Figure 48 shows an example taken from March 2009 where the operational monthly forecast failed to predict the fast propagation of the MJO after about 15 days. Instead the convection in the model is stationary over the Maritime continent until the end of the forecast. As a result, the precipitation anomalies predicted over eastern Indonesia and Australia for day 26-32 were opposite to the analysis (Fig. 49): in the model, the positive phase of the MJO was still over the Maritime Continent, when a negative phase of the MJO should have already moved over that area according to ERA Interim.

The MJO teleconnections are well captured by the model in the Tropics. For instance, the impact of the MJO on the precipitation over South America, Equatorial Africa and on tropical cyclogenesis are very consistent with reanalysis. In the Extratropics, the model teleconnections are generally consistent with ERA Interim, except over Europe where the impact in the model seems too weak, although the model simulates a statistically significant impact on the positive phase of the NAO. The too slow propagation of the MJO could explain part of the too weak impact of the MJO over Europe, but as mentioned above there is considerable uncertainty about the impact of the MJO over Europe.

Finally, the impact of the MJO on the forecast skill was investigated. Results show that the MJO has no significant impact for the period day 5-11, but has a significant positive impact for day 12-18, 19-25 and 26-32. The day 19-25 period is particularly interesting with the model showing almost no skill at all when there is no MJO in the initial conditions, but the forecasts become reliable and skilful when there is an MJO in the initial conditions. This could represent a very useful information for the users of the monthly forecasting system, which can use the presence of an MJO event in the initial conditions to have an a priori estimate of the skill of the day 19-25 forecasts.

7 References

Bechtold., P., M. Koehler, T. Jung, P. Doblas-Reyes, M. Leutbecher, M. Rodwell and F. Vitart, 2008: Advances in simulating atmospheric variability with the ECMWF model: From synoptic to decadal time scales, *Quart. J. R. Meteorol. Soc.*, **134**, 1337-1351.

Cassou, C., 2008: Intraseasonal interaction between the Madden-Julian Oscillation and the North Atlantic Oscillation. *Nature*, doi:10.1038/nature07286.

Ferranti, L., T. N. Palmer, F. Molteni and E. Klinker, 1990: Tropical-extratropical interaction associated with the 30-60 day oscillation and its impact on medium and extended range prediction. *J. Atm. Sci.*, **125**, 2177-2199.

Hendon, H. H. and B. Liebmann, 1990: A composite study of onset of Australian summer monsoon. J. Atmos. Sci., **48**, 2909-2923.

Jones, C., D. Waliser, K. Lau and W. Stern, 2004: The Madden-Julian Oscillation and its impact on Northern Hemisphere weather predictability. *Mon. Wea. Rev.*, **132**, 1462-1471.

Jung, T. and Palmer, T., 2009: Diagnosing the origin of extended-range forecast error. *Submitted to Mon. Wea. Rev.*.

Kessler, K. S. and M. J. McPhaden, 1995: Oceanic equatorial Kelvin waves and the 1991-1993 El-Niño. *J. Climate*, **8** 1757-1774.

Madden, R. A. and P.R. Julian, 1971: Detection of a 40-50 day oscillation in the zonal wind in the tropical Pacific. *J. Atm. Sci.*, **5**, 702-708.

Maloney, E. D. and D. L. Hartmann, 2000a: Modulation of Eastern North Pacific Hurricanes by the Madden-Julian Oscillation. *J. Climate*, **13**, 1451-1460.

Maloney, E. D. and D. L. Hartmann, 2000b: Modulation of hurricane activity in the Gulf of Mexico by the Madden-Julian Oscillation, *Science*, **287**, 2002-2004.

Mo, K.C., 2000: The association between intraseasonal oscillation and tropical storms in the Atlantic basin. *Mon. Wea. Rev.*, **128**, 4097-4107.

Murakami, T., 1976: Cloudiness fluctuations during the summer monsoon, *J. Meteor. Soc. of Japan*, **54**, 175-181.

Simmons, A., S. Uppala, D. P. Dee and S. Kobayashi, 2007: ERA-Interim: New ECMWF reanalysis products from 1989 onwards, *ECMWF Newsletter*, **110**, 25-35.

Vitart, F, 2004: Monthly forecasting at ECMWF. Mon. Wea. Rev., **132**, 2761-2779.

Vitart, F., S. Woolnough, M.A. Balmaseda and A. Tompkins, 2007: Monthly forecast of the Madden-Julian Oscillation using a coupled GCM. Mon. Wea. Rev., 135, 2700-2715.

Vitart, F., R. Buizza, M. Alonso Balmaseda, G. Balsamo, J.-R. Bidlot, A. Bonet, M. Fuentes, A. Hofstadler, F. Moleni and T. Palmer, 2008: The new VAREPS-monthly forecasting system: a first step towards seamless prediction. *Quart. J. Roy. Meteor. Soc.*, **134**, 1789-1799.

Vitart, F. and F. Molteni, 2009: Dynamical extended-range prediction of early monsoon rainfall over India. *Mon. Wea. Rev.*,**137**,1480-1492.

Vitart, F., 2009: Impact of the Madden Julian Oscillation on tropical storms and risk of landfall in the ECMWF forecast system. *Geophys. Res. Lett.*, L15802, doi:10.1029/2009GL039089.

Weigel, A., D. Baggenstos, M.A. Liniger, F. Vitart and C. Appenzeller, 2008: Probabilistic verification of monthly temperature forecasts. *Mon. Wea. Rev.*, **136**, 5162-5182.

Wheeler, M.C. and H.H. Hendon, 2004: An all-season real-time multivariate MJO index: Development of an index for monitoring and prediction. *Mon. Wea. Rev.*, **132**, 1917-1932.

Woolnough, S.J., F. Vitart and M.A. Balmaseda, 2007: The role of the ocean in the Madden-Julian Oscillation: Implications for MJO prediction. *Q. J. R. Meteorol. Soc.*, **133**, 117-128.

Yasunari, T., 1979: Cloudiness fluctuations associated with the Northern Hemisphere summer monsoon. *J. Meteor. Soc. of Japan*, **58**, 225-229.